RSC Advances

REVIEW

View Article Online
View Journal | View Issue

Cite this: *RSC Adv.*, 2026, **16**, 14575

Sustainable catalytic conversion of ethanol: catalyst design and modification strategies for dehydration and petrochemical applications

Rasha S. Mohamed *[a] and Heba M. El Sharkawy *[b]

Received 8th January 2026
Accepted 10th March 2026

DOI: 10.1039/d6ra00209a

rsc.li/rsc-advances

Ethanol has emerged as a promising renewable feedstock for chemicals and sustainable fuel production. Its conversion into ethylene, diethyl ether, and higher-value chemicals through dehydration over catalysts relies on carefully designed catalysts to enhance activity, selectivity, and stability. This review critically examines the catalytic transformation pathways leading to key petrochemical intermediates such as ethylene, propylene, and 1,3-butadiene. It places special emphasis on solid acid catalysts, modified oxides, zeolites, and heteropoly acids, highlighting recent advances in catalyst design, including surface modification, morphology control, and nanostructuring. The review also discusses mechanistic insights, reactor engineering, and strategies to overcome coke formation and catalyst deactivation. Finally, it explores future perspectives on integrating bioethanol into petrochemical supply chains, focusing on challenges related to catalyst performance, process scalability, and sustainable chemical production.

1. Introduction

The global use of ethanol as an alternative engine fuel has steadily risen due to its potential to decrease dependence on fossil fuels, enhance energy security, generate rural employment, and reduce air pollution and greenhouse gas emissions.[1–5] Over the past two centuries, industrial development has significantly contributed to environmental pollution, leading to contamination of air, water, and soil.[6–8] Notably, the concentration of atmospheric CO_2 has surged, with an estimated 38 000 million metric tons added over the last 260 years, primarily due to fossil fuel consumption.[9–11]

[a]*Refining Division, Egyptian Petroleum Research Institute (EPRI), 1 Ahmed El-Zomor St., Nasr City, 11727, Cairo, Egypt. E-mail: rashaepri2009@yahoo.com*
[b]*Department of Analysis and Evaluation, Egyptian Petroleum Research Institute (EPRI), Cairo, Egypt. E-mail: h_magdy54@yahoo.com*

Rasha S. Mohamed

Dr Rasha El-Sayed Mohamed is an Assistant Professor of Applied Physical Chemistry at the Egyptian Petroleum Research Institute (EPRI), currently seconded to the Central Laboratory for Liquid Chromatographic and Water Analysis. She received her PhD in Applied Physical Chemistry from Ain Shams University in 2015 and her MSc in Inorganic Chemistry from Helwan University in 2008. Her research focuses on the synthesis of advanced catalysts, including nano metal oxides and metal–organic frameworks, for petroleum refining, photocatalysis, hydrogen production and storage, water treatment, and diesel desulfurization. She holds two Egyptian national patents (no. 31340 and 31186) and received the Knowledge Medal from the American International Academy for Higher Education.

Heba M. El Sharkawy

Dr Heba Magdy El Sharkawy is a researcher at the Egyptian Petroleum Research Institute and a research assistant at the Energy Materials Lab, American University in Cairo. She earned her Ph.D. in Physical Chemistry from Al-Azhar University (2021), focusing on carbon quantum dots for energy storage and photocatalytic pollutant degradation. Her research spans supercapacitor development, sustainable energy applications, water treatment, materials science and green fuel production. Dr El Sharkawy has authored numerous peer-reviewed publications in energy and environmental materials and received the 2024 Dr Ferdous Abdel-Majeed Award for her contributions to new and smart materials.

This trend not only jeopardizes environmental sustainability but also restricts access to these non-renewable resources for future generations. Therefore, transitioning to renewable and alternative fuels is crucial for minimizing environmental impact and meeting global energy demands.[12–14] Ethanol stands out as one of the most significant biofuels, thanks to its oxygen content (~35%), which helps reduce particulate and NO_x emissions compared to gasoline.[15–18] As illustrated in Fig. 1, ethanol can be produced through two primary pathways: chemical routes from fossil fuels and biological routes from biomass.[19] Ethanol can be produced not only from petroleum and biomass but also from coal through a two-step process: gasification followed by catalytic conversion of syngas ($CO + H_2$) into ethanol. This thermochemical pathway is a significant non-biological method, especially in coal-rich areas, and has garnered growing interest as a component of integrated carbon utilization strategies.[19] The chemical (petrochemical) route involves producing ethanol from petroleum-based feedstocks, while the biological route utilizes renewable biomass, making bioethanol production more sustainable and eco-friendly.[20,21]

Beyond its role as a fuel, ethanol also serves as an important platform molecule for catalytic conversion into value-added chemicals, including ethylene, higher alcohols, and other petrochemical intermediates.[22–24] Many studies focus on individual catalysts or reaction pathways; however, a comprehensive evaluation is needed to critically compare catalyst design, modification strategies, and reaction mechanisms.[25] The development of efficient and selective catalysts is therefore essential for improving ethanol conversion processes while ensuring sustainability and economic viability.[26,27] This review aims to provide a critical assessment that highlights recent advancements, as well as current limitations, challenges, and research gaps, thereby offering guidance for future development in the field.

2. Bioethanol production

Bioethanol is poised to be a leading fuel of the future, as it is derived from renewable sources, specifically biomass, and is environmentally friendly.[28,29] Ethanol enhances the octane rating of gasoline, acts as an anti-knock agent, and has the potential to replace current fuel additives,[30] as illustrated in Fig. 2. With the rising cost of petroleum, the production of ethanol can be doubled, while petrochemical routes decline.[19,31] Currently, the production of ethanol from biomass is becoming more efficient and competitive, resulting in a lower-cost end product. At present, 90 percent of the ethanol market is generated from biomass.[32–34] The global ethanol market, depicted in Fig. 2, shows production trends across major producing countries. Projections for 2025 indicate that the global ethanol market value will exceed USD 114 billion, reflecting strong industry growth and increasing integration of ethanol into the energy and transport sectors.[35,36] By 2028, it is expected that more than half of ethanol production will be consumed by high-speed flexible fuel vehicles, indicating anticipated fleet expansion.[37,38]

Ethanol can be synthetically produced from biomass resources through fermentation, either using oil or microbial processes. This fermentation of sugar typically involves three phases: (1) developing a fermented sugar solution; (2) fermenting the ethanol; and (3) separating and purifying the ethanol, usually through distillation.[29,40] As an attractive alternative to traditional fossil fuel-derived raw materials in petrochemical production, ethanol's conversion into higher-value chemicals, such as ethylene, relies heavily on optimizing the catalyst and process to accommodate ethanol's unique properties.[41]

3. Ethanol as a substrate for bulk chemicals

Ethanol can be transformed into commercial chemicals through chemical or fermentation processes. However, the

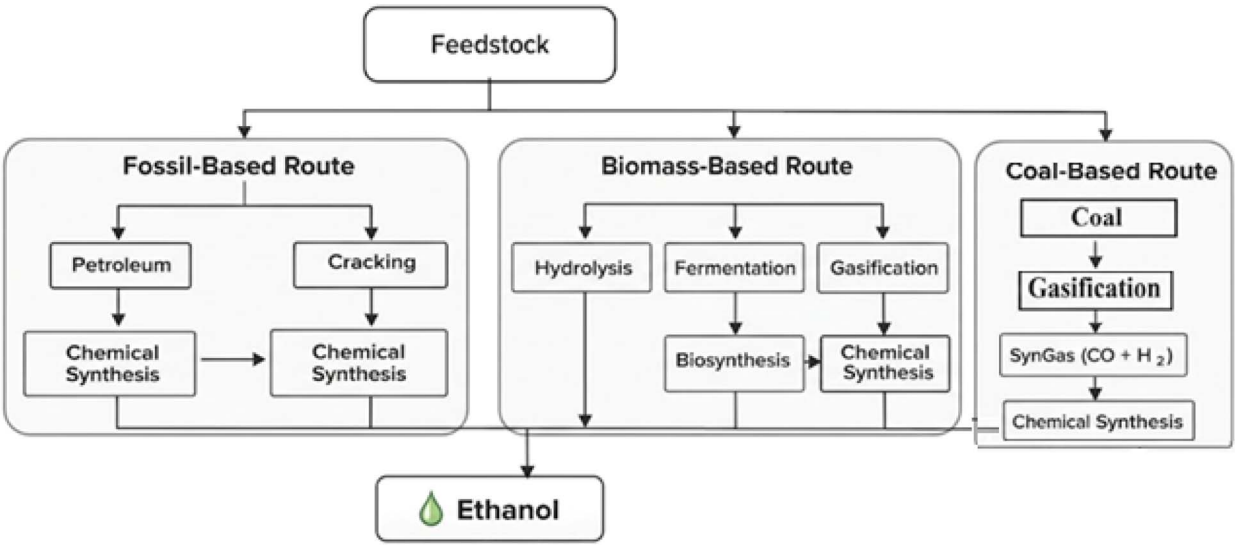

Fig. 1 Overview of the ethanol production pathways.

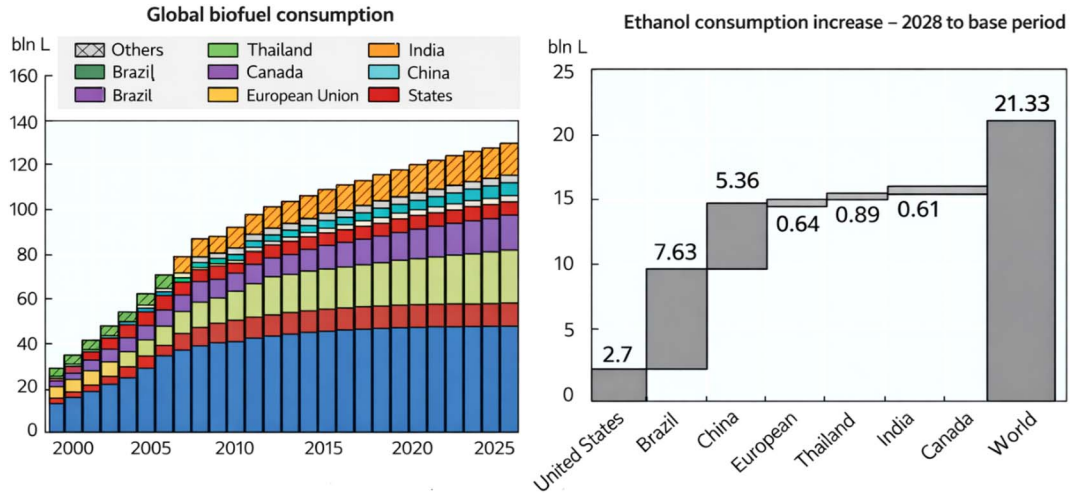

Fig. 2 Global ethanol production and market trends (million m^3). Adapted from ref. 39.

COVID-19 pandemic led to a decrease in ethanol production, dropping to 26 billion gallons in 2020.[42] Despite this decline, the United States remained the world's largest producer, responsible for over half of global output[43] (Fig. 3).

Recent advancements in new technologies and strategic partnerships have enhanced the potential of ethanol as a platform molecule for chemical synthesis. Ethanol can be converted into a variety of significant bulk compounds,[22] as illustrated in Fig. 4. It's crucial to highlight that ethanol can also function as a chemical platform molecule, allowing for the catalytic transformation into essential industrial chemical components using multifunctional catalysts in single-stage catalytic processes.[45] Chemicals such as acetic acid, ethyl chloride, acetic anhydride, cellulose acetates, ethyl ether, acetaldehyde, acetone, butanol, ethylene, and propylene all contribute to the production of acetone, which is already being manufactured in Brazil.[46] Additionally, the synthesis of 1,3-butadiene rubber monomer from ethanol was a viable business technology in Brazil in the past. However, the ethanol chemical industry has not received the same level of investment and technological development as the petrochemical sector; it was largely neglected in the 1990s and has not fully recovered.[47] In 2010, Braskem emerged as the leading producer of bio-based polyethylene from ethanol in Brazil.[48]

Given the potential for increased ethanol production and the ongoing shift towards electric vehicles, there is significant opportunity for revitalizing the ethanol chemical sector in Brazil.[49] The manufacturing of ethylene, which is the most advanced process for producing plastics, can be achieved through the dehydration of ethanol. While ethanol can also be converted into heavier fuels like jet fuel and used in the steam reforming of ethanol for strategic hydrogen production, its potential as a platform molecule remains substantial.[50]

4. Dehydration of ethanol

The catalytic dehydration of ethanol is a crucial reaction for producing ethylene using solid acid catalysts. The primary process involves the intramolecular dehydration of ethanol, resulting in the formation of ethylene and water.[51] Additionally,

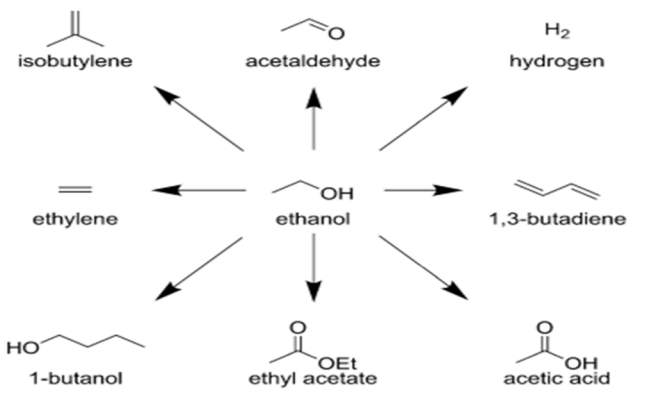

Fig. 3 Major industrial chemicals derived from ethanol as a platform molecule (reprinted with permission,[44] copyright 2013 John Wiley and Sons).

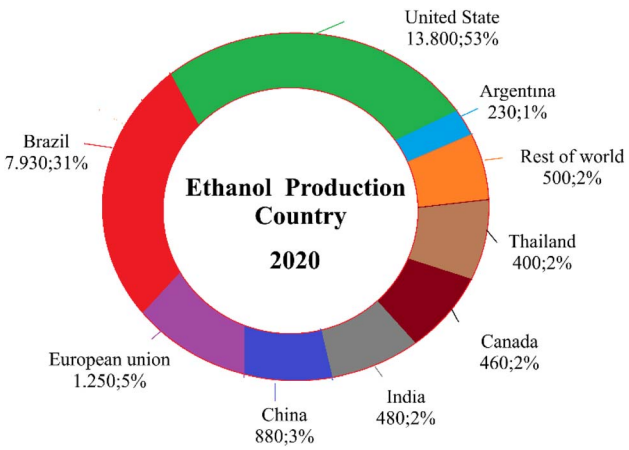

Fig. 4 Global ethanol production by country (country, million gallons).

ethanol can undergo intermolecular dehydration to produce diethyl ether, which can decompose into ethylene at higher temperatures. The selectivity between ethylene and diethyl ether is strongly influenced by the reaction temperature and the acidity of the catalyst.[52] Typically, diethyl ether formation is favored at lower temperatures, while ethylene becomes the predominant product at higher temperatures.[53] Side reactions may also occur, depending on the catalyst properties and operating conditions, leading to the formation of minor amounts of acetaldehyde and light hydrocarbons. Therefore, factors such as catalyst acidity, reaction temperature, pressure, and liquid hourly space velocity (LHSV) are critical in controlling product distribution and minimizing by-product formation.[54]

In industrial applications, solid acid catalysts like alumina are commonly used, usually operating at moderate temperatures between 200 and 300 °C. The performance of the catalyst and the purity of the ethanol feed significantly affect conversion efficiency and product selectivity.[55]

4.1. Ethylene

4.1.1. Properties of ethylene. Ethylene (C_2H_4) is the simplest alkene and a highly reactive olefin due to its carbon–carbon double bond (C=C).[56] This π-bond creates a high electron density, making ethylene prone to electrophilic addition and polymerization reactions. These chemical properties highlight its significant industrial importance and its role as a key target product in ethanol dehydration processes.[57] In catalytic systems, ethylene interacts with transition metal surfaces through temporary coordination with its π and π* orbitals, which is crucial for subsequent transformations. Therefore, understanding ethylene's reactivity is essential for evaluating routes for converting ethanol to ethylene.[58]

4.1.2. Importance and applications of ethylene. Ethylene ranks among the highest-volume petrochemicals in the world, serving as a key building block for various products including polyethylene, ethylene oxide, ethylene glycol, and polyvinyl chloride (PVC).[59–61] Notably, polyethylene constitutes nearly 60% of global ethylene consumption. The persistent global demand for these derivatives underscores the strategic importance of developing sustainable ethylene production methods.[62,63] Traditionally, ethylene has been produced from ethanol through catalytic dehydration, and modern industrial processes have demonstrated the viability of generating high-purity ethylene from bioethanol, highlighting the potential of renewable feedstocks.[64]

4.1.3. Ethylene production. The manufacture of ethylene can be achieved through several well-known methods, including: (i) cracking of higher hydrocarbons, (ii) plant-based production, (iii) microbial synthesis and (iv) catalytic dehydration of ethanol.

Fig. 5 illustrates the various industrial methods for ethylene production.[65] Although the cracking of higher hydrocarbons is still the primary petrochemical route, ethanol dehydration has become a significant renewable alternative, enabling bioethanol to function as a platform molecule for sustainable ethylene production.[66] While plant-based and microbial processes are not yet widely adopted in industry, they offer promising avenues for future bio-based ethylene production.[67]

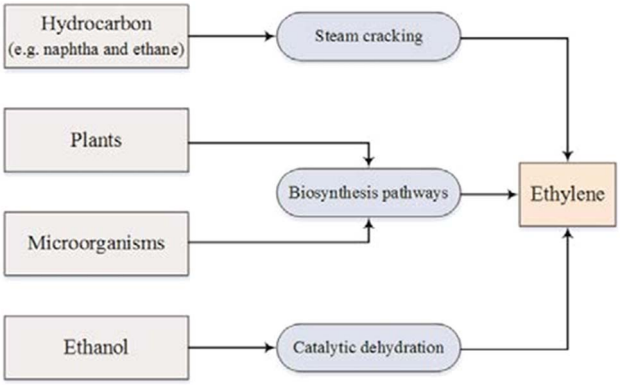

Fig. 5 Schematic diagram for several ethylene manufacturing processes (reprinted with permission,[68] copyright 2017 John Wiley and Sons).

4.1.3.1. Steam cracking of hydrocarbons. Steam cracking of liquefied petroleum gas (LPG) or heavier hydrocarbons is the primary industrial method for producing ethylene.[69,70] This process operates at high temperatures (750–850 °C) in the absence of oxygen and requires substantial energy input. Despite being an established technique, it encounters challenges, including catalyst deactivation from carbon deposition, by-product formation, and high operational costs due to the extreme temperatures involved.[71] Additionally, fluctuations in petroleum prices and growing environmental concerns have spurred the search for alternative, renewable methods of ethylene production.[72]

4.1.3.2. Ethylene production by plants. Ethylene is a phytohormone naturally produced in plants, playing a crucial role in regulating processes such as fruit ripening.[73] Its biosynthetic pathway involves the enzymes ACC synthase (ACS) and ACC oxidase (ACO), which convert *S*-adenosyl methionine (SAM) into ethylene. However, the production scale is currently very limited and not viable for industrial applications.[74]

4.1.3.3. Ethylene production by microorganisms. Certain bacteria and fungi can produce ethylene. Despite the scientific interest in microbial ethylene biosynthesis, the production yields are insufficient for large-scale industrial use.[65]

4.1.3.4. Ethylene production by catalytic dehydration of ethanol. Catalytic dehydration of ethanol presents a promising alternative to steam cracking due to its lower operating temperature and compatibility with renewable feedstocks.[75,76] Unlike hydrocarbon cracking, ethanol can be sourced from biomass, making this process independent of fossil resources.[77]

The overall dehydration reactions are as follows:

$$C_2H_5OH \Rightarrow H_2O + C_2H_4,\ +44.9\ \text{kJ mol}^{-1} \quad (1)$$

$$C_2H_5OH \Rightarrow 0.5C_2H_5OC_2H_5 + 0.5H_2O,\ -12\ \text{kJ mol} \quad (2)$$

$$C_2H_5OC_2H_5 \Rightarrow 2C_2H_4 + H_2O,\ +115\ \text{kJ mol}^{-1} \quad (3)$$

At elevated temperatures, the reaction is endothermic and may occur through both direct ethanol dehydration and sequential dehydration *via* diethyl ether as an intermediate. Additionally, side reactions can produce acetaldehyde, methane, ethane, propylene, CO, CO_2, and H_2.[55] Compared to steam cracking plants, catalytic ethanol dehydration requires significantly lower capital investment and provides environmental benefits. Therefore, this method represents a sustainable and economically attractive alternative for future ethylene production.[78]

4.1.4. Global market for ethylene. Ethylene is one of the highest-volume petrochemicals globally and serves as a fundamental building block in the chemical industry.[79] The largest share of ethylene consumption is attributed to polyethylene, followed by ethylene oxide and polyvinyl chloride, as shown in Fig. 6. The ongoing global demand for these derivatives highlights the strategic importance of securing reliable and diverse production routes.[64] Recent market fluctuations, particularly during the COVID-19 pandemic, have revealed the vulnerability of ethylene supply chains to global economic and energy disruptions. This volatility underscores the necessity of complementing traditional steam cracking with alternative and renewable production methods.[80] In this context, the catalytic dehydration of bioethanol presents a promising strategy to reduce reliance on fossil resources while ensuring a steady supply of essential ethylene-derived products.[81]

4.2. Diethyl ether

4.2.1. Properties of diethyl ether. Diethyl ether, with the chemical formula $(C_2H_5)_2O$, belongs to the ether class. It is highly volatile, has an octane number greater than 125 or 110, is extremely colorless, possesses a suitable energy density for onboard storage, has a high concentration of oxygen, a low autoignition temperature, broad flammability limits, and high miscibility with diesel and ethanol fuels.[82]

4.2.2. Importance and applications of diethyl ether. Diethyl ether is commonly used as a solvent in various fine chemistry, fragrance, and pharmaceutical processes, as well as a starting fluid in some engines. It was previously utilized as a general anesthetic until non-flammable agents like halothane were introduced. Additionally, it has been misused as a recreational drug. The production of diethyl ether is significant due to its role as a major product in the chemical industry.[83] It has numerous applications in the fuel chemical industry, enhancing combustion in both diesel and gasoline engines. Research has explored the partial conversion of ethanol to diethyl ether to improve ethanol volatility during cold starts, similar to gasoline.[82] However, its high volatility, poor lubricity, and anesthetic effects present notable drawbacks.[84]

5. Reactor types for the catalytic dehydration of ethanol

Ethanol dehydration occurs during the vapor phase in reactors, either fixed bed or fluidized bed, that contain a catalyst. In fluidized bed reactors, the process can be isothermal or adiabatic, although most cases tend to be adiabatic.[85]

5.1. Fixed-bed reactors

Fixed-bed reactors consist of several thousand long, thin tubes housed within a vessel. Each tube, approximately 2–3 mm in diameter, contains catalyst particles. These reactors also function as heat exchangers, generating steam on the outer side of the tubes during the Fischer–Tropsch reaction.[85] A schematic diagram of the fixed-bed reactor is presented in Fig. 7. While fixed-bed reactors are simple, adaptable, and scalable, they have several drawbacks. These include high costs and the requirement for multiple reactors in tandem for large-scale operations. Additionally, large catalyst particles are necessary to avoid significant pressure drops within the reactor tubes, which can

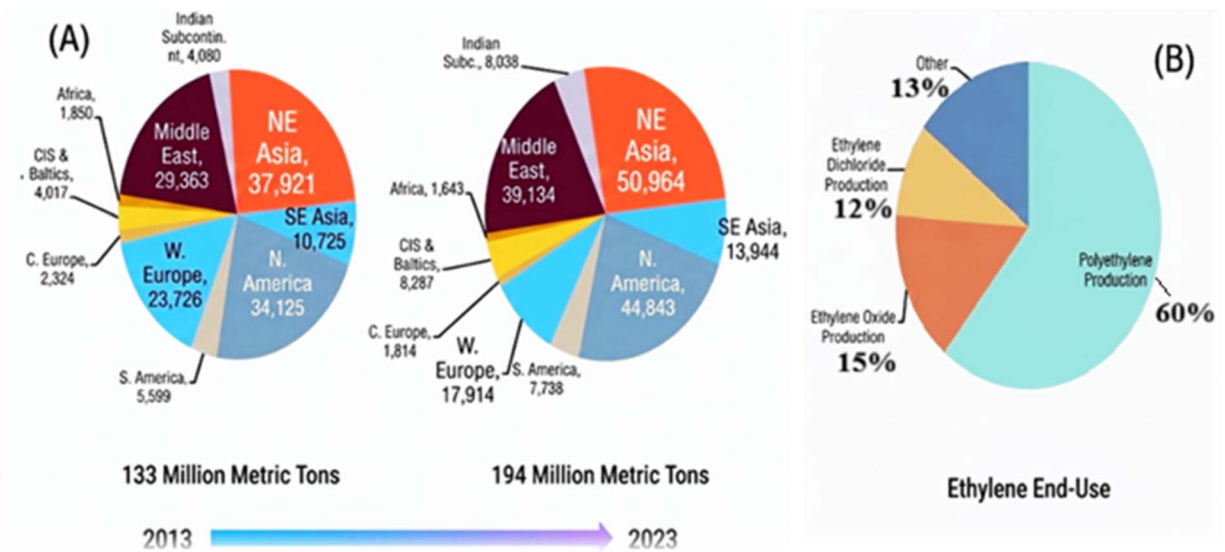

Fig. 6 World ethylene demand (A) and demand distribution by application (B).

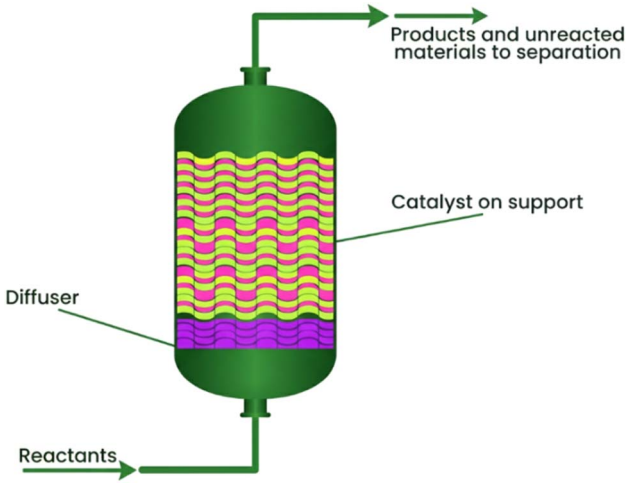

Fig. 7 Schematic diagram of fixed bed reactor. Adapted from ref. 88.

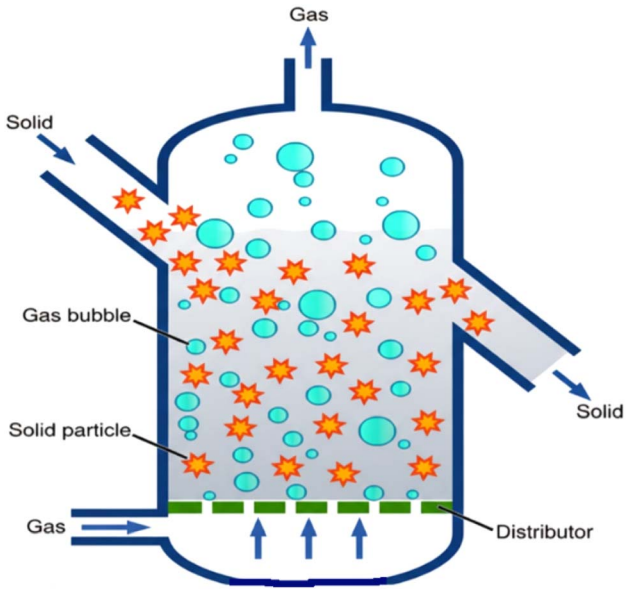

Fig. 8 Basic diagram of fluidized bed reactor. Adapted from ref. 92.

lead to reduced effectiveness. This is due to low catalyst activity per unit mass, resulting from the difficulty of reactants diffusing into the core of the catalyst particles.[86,87]

5.1.1. Fixed-bed isothermal reactor. The isothermal technique is commonly used for the dehydration of ethanol. This process typically employs a multi-tubular fixed bed system, where the catalyst is contained within the tubes.[67] For the endothermic reaction, a thermal stream circulates on the shell side, operating at temperatures between 330 and 380 °C, with a liquid hourly space velocity (LHSV) of approximately 0.2 to 0.4 h^{-1}. This setup achieves ethanol conversion rates of 98–99%, with molar selectivity for ethylene reaching 95–99%. Regular catalytic regeneration is necessary due to coke deposition, which involves using air diluted with steam every 1 to 6 months, depending on the catalyst and the specific procedure. Managing the temperature in larger tubes can be challenging, which limits the scalability of the process.[87]

5.1.2. Adiabatic fixed-bed reactor. In this procedure, a series of fixed-bed reactors filled with catalyst are used. An inert heat-carrying fluid supplies the necessary heat for the process. The feed stream, entering each subsequent reactor, is reheated by intermediate heating units. The typical steam-to-ethanol ratio in the input stream ranges from 2 : 1 to 3 : 1, with ethanol make-up streams added between each stage. The LHSV is around 0.15 to 0.5 h^{-1}, and the inlet temperature is maintained at 450–500 °C. This setup achieves conversion rates exceeding 99%, with ethylene molar selectivity between 97% and 99%. The catalyst regeneration cycle occurs every 6 to 12 months due to steam usage and coke production.[69,89]

5.2. Fluidized-bed reactor

A fluidized bed reactor (FBR) is a versatile device designed for various multiphase chemical reactions. In this type of reactor, a fluid (gas or liquid) is passed through a solid catalyst at high speeds, suspending the solid and enabling it to behave like a fluid. This process, known as fluidization, offers several significant advantages, overcoming various operational challenges.[90] The FBR demonstrates greatly improved mass and heat transfer and reduced temperature gradients. The effective mixing of the catalyst with the fluid increases the surface area available for reactions, enhancing mass and heat transfer. Fig. 8 showed a schematic diagram of a fluidized-bed reactor.[91] The fluidized bed reactor facilitates near-complete ethanol conversion with exceptionally high selectivity for ethylene. Optimal temperature control minimizes by-product formation and coke accumulation. At 400 °C, ethanol is converted to ethylene with a conversion rate of 99.5% and a molar selectivity of 99.9%. The endothermic heat required for the reaction is supplied by the hot fluid and the heated catalyst, which is recycled from the catalyst regenerator.[65]

In conclusion, fixed-bed reactors achieve high conversion rates of ethanol (approximately 98–99%) and high selectivity for ethylene (95–99%). Their mechanical simplicity and low cost make them suitable for low to medium production volumes.[93] However, challenges such as temperature gradients within the reactors, carbon deposit accumulation on catalyst surfaces, and the necessity for periodic catalyst regeneration limit their long-term performance and flexibility for large-scale applications. Additionally, adiabatic configurations require extra energy to heat the catalysts to the reaction temperature and to ensure adequate steam dilution.[94] In contrast, fluidized bed reactors offer enhanced heat and mass transfer characteristics, ensuring uniform temperature distribution and minimizing hot spot formation.[95] They also allow for continuous catalyst regeneration, which improves overall reactor operation and achieves a very high selectivity (>99%) for ethylene production. As a result, fluidized systems are generally more appealing than fixed systems for large-scale continuous production processes. However, they require a higher capital investment and more complex operational control compared to fixed beds.[96]

6. Process for catalytic dehydration of ethanol

An industrial facility has been approved by the SINOPEC Shanghai Research Institute of Petrochemical Technology (SRIPT) for the dehydration of ethanol to ethylene (ETE).[97] In the ethanol-to-ethylene (ETE) industrial process, reactors facilitate the reaction between ethanol and catalysts, resulting in the formation of ethylene gas.[98] This occurs through both intermolecular and intramolecular dehydration of ethanol molecules. Lewis acid sites on the catalyst surface promote intermolecular dehydration, while Brønsted acid sites facilitate intramolecular dehydration. Typically, in a fixed bed reactor, Brønsted acid sites drive reactions within a temperature range of 350° to 450 °C. Below 350°, intermolecular dehydration between two ethanol molecules produces diethyl ether. Consequently, catalyst properties significantly influence catalytic selectivity, coke generation, and the operational lifespan of the catalyst.[99]

To optimize the reaction, the fixed bed reactor operates in conjunction with an isothermally-operated reboiler, ensuring efficient heat transfer during the endothermic reaction and promoting uniform catalytic activity throughout the catalyst bed. Although downstream equipment such as a water scrubber, alkaline wash column, dryer, or stripper does not directly influence the catalytic process, it can improve overall catalyst performance by removing acidic gases, water, and heavier hydrocarbons that might disrupt the reaction equilibrium and lead to catalyst poisoning. Thus, the overall process engineering integrates both catalysis and separation operations, ensuring sustained high selectivity for ethylene production from the ethanol feed while prolonging catalyst life.[100]

This process employs an isothermal fixed-bed reactor along with two low-temperature separation columns, a water scrubber, and an alkaline wash column, as depicted in Fig. 9. Ethanol conversion achieves 99%, with ethylene selectivity exceeding 96% at reaction temperatures of 350–450 °C and a liquid hourly space velocity (LHSV) of 0.5–1.0 h^{-1}. The catalyst has an operational lifetime of approximately one year.[68] This method is not only economical and practical but also environmentally friendly. The ethanol feed is vaporized and preheated using the reactor effluent before entering the reactor. Gases exiting the scrubber are directed to the alkaline wash column, which consists of two sections: the lower alkaline section removes acidic gases (*e.g.*, CO_2) using a recycled diluted alkaline solution, while the upper water-scrubbing section further eliminates residual acidic gases. The rough ethylene stream is then compressed, cooled, and dried before entering the ethylene column, where ethane, C_3 compounds, and other heavier components are separated. Finally, the stream passes through a stripper to eliminate light gases such as H_2, CH_4, and CO, yielding high-purity ethylene collected at the base of the stripper for storage.[101]

7. Reaction mechanism of ethanol dehydration

The reaction mechanism for the dehydration of ethanol is depicted in Fig. 10. In this process, ethylene is primarily formed at Brønsted acid sites, while diethyl ether is predominantly produced at Lewis acid sites.[103,104]

Fig. 11 illustrates the mechanism of ethanol dehydration over acid catalysts to produce ethylene. The process begins with the protonation of the hydroxyl group oxygen atom in ethanol, which enhances its ability to leave. Next, the loss of a water molecule occurs, creating carbocation intermediate. Finally, the deprotonation of the carbon atom adjacent to the carbocation

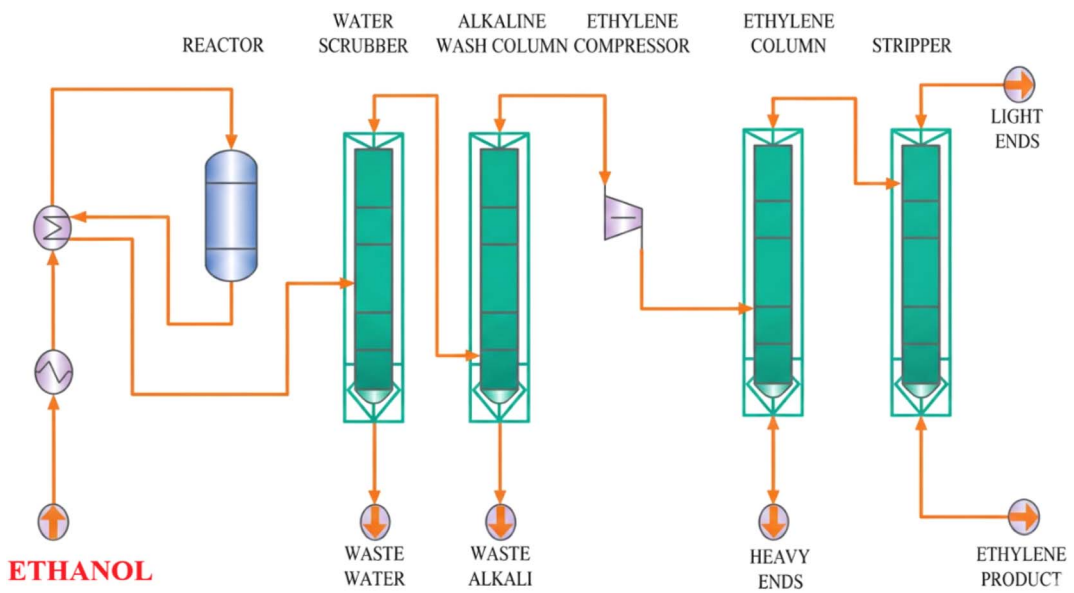

Fig. 9 Schematic diagram of the ethylene production process *via* ethanol dehydration. Adapted from ref. 102.

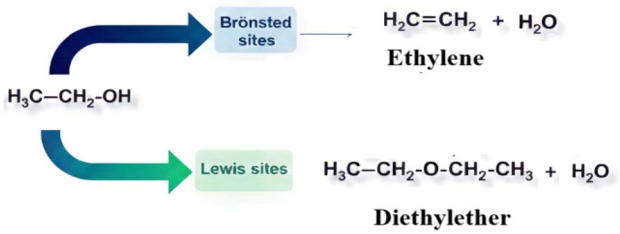

Fig. 10 Reaction network of ethanol dehydration over catalyst.

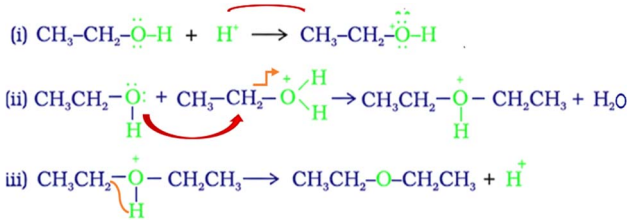

Fig. 11 Dehydration mechanism of ethanol to ethylene. Adapted from ref. 107.

results in the formation of a carbon–carbon double bond, producing ethylene.[105,106]

The reaction to form diethyl ether proceeds *via* a unimolecular nucleophilic substitution pathway. Initially, ethanol is treated with an acid catalyst that generates protons, enabling the elimination of a water molecule from one ethanol molecule, which results in the formation of a carbocation. Next, a second ethanol molecule acts as a nucleophile and attacks the electrophilic carbon of the carbocation.[108] This unimolecular nucleophilic substitution ultimately produces diethyl ether, as shown in Fig. 12.

8. Catalysts for dehydration of ethanol

Acid catalysts are typically used in the dehydration of ethanol. Sulfuric acid and phosphoric acid are the standard homogeneous catalysts employed in nearly every industrial process.[109] This reaction generally requires high temperatures, leading to reduced ethylene selectivity and coke deposition, which deactivates the catalyst.[59] As a result, these acids fell out of favor as early as 1995.[110] Solid acid heterogeneous catalysts, on the other hand, are more environmentally friendly, less corrosive, and generate less waste than their homogeneous counterparts, which often suffer from poor yields. These solid catalysts are also more stable and resilient to sulfuric and phosphoric acids, and they are easier to separate from the reaction mixture.[111]

8.1. Design strategies for catalysts used in ethanol dehydration

Metal oxides are frequently used as solid acid catalysts for ethanol dehydration due to their Lewis acidic (metal atoms) and Brønsted acid sites (oxygen atoms), which influence both ethylene selectivity and catalyst stability. The dehydration reaction requires the production of 390 calories of ethylene per gram.[75] To improve catalytic performance, various preparation techniques have been developed to precisely control particle size, morphology, crystallinity, and chemical composition, all of which directly impact ethanol conversion efficiency and catalyst longevity.[112,113] These techniques are generally categorized into bottom-up approaches, where nanoparticles are assembled from atoms or molecules using methods such as chemical synthesis, sol–gel processes, colloidal assembly, and self-assembly, and top-down approaches, in which bulk materials are reduced to nanoscale through processes like deposition, etching, nano-lithography and mechanical treatments modify surface-to-volume ratios, enhancing catalytic activity. Both gas–solid methods, such as chemical vapor deposition and pulsed laser deposition, and liquid–solid methods, including co-precipitation, solvothermal synthesis, sonication, and microwave-assisted preparation, are used to optimize metal oxide catalysts for ethanol-to-ethylene conversion.[114,115] These techniques aim to maximize selectivity while minimizing coke formation. Fig. 13 illustrates the general concepts of bottom-up and top-down preparation.[114]

8.1.1. Catalyst preparation strategies and their impact on ethanol dehydration performance. The methods used for catalyst preparation significantly affect their physicochemical

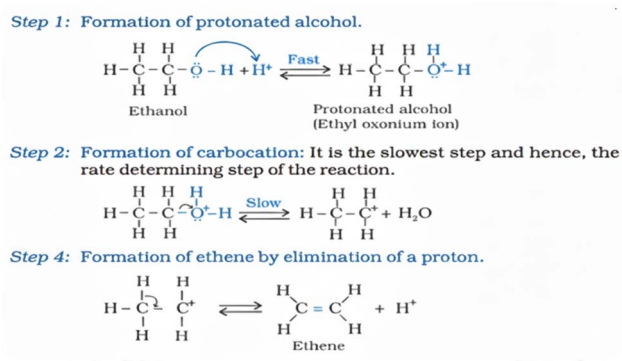

Fig. 12 Formation of diethyl ether from ethanol. Adapted from ref. 107.

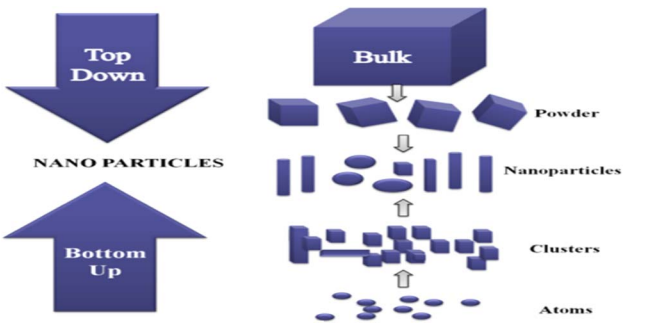

Fig. 13 Nanoparticular oxide production methods[116] (DOI: https://doi.org/10.3390/nano12193465, Open-source: MDPI).

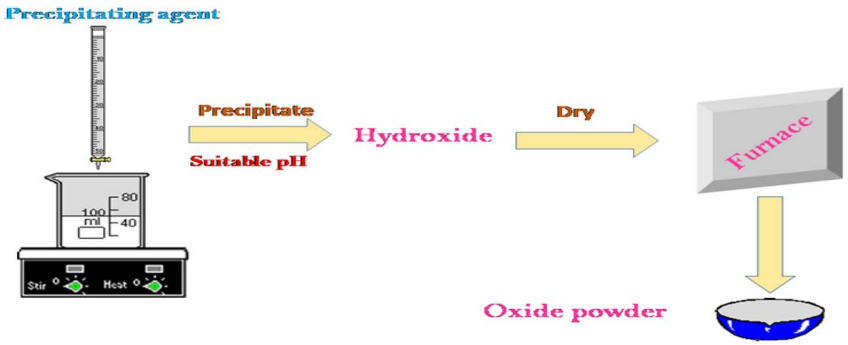

Fig. 14 Schematic of co-precipitation for ethanol dehydration catalysts[125] (DOI: https://doi.org/10.32628/IJSRST, Open-source: ICRTMS-2024 International).

properties and, in turn, the performance of ethanol dehydration.[117] Co-precipitation techniques result in moderate surface area and uniform metal distribution, which provide balanced Lewis acidity, but they offer limited control over pore structure and moderate resistance to coke formation.[118] Sol–gel methods improve homogeneity and allow for tunable acidity, enhancing the accessibility of acid sites and increasing ethylene selectivity, although scaling up these processes can be challenging.[119] Hydrothermal synthesis enhances crystallinity and structural stability, which leads to improved diffusion, hydrothermal resistance, and a longer catalyst lifetime, though at a higher cost.[120] Techniques such as microemulsion, microwave-assisted synthesis, and sonochemical methods generally produce smaller particles and better dispersion, which enhance the availability of active sites and catalytic activity, but they face limitations in industrial scalability.[121] Overall, synthesis strategies that optimize acidity, porosity, and metal–support interactions tend to promote higher ethylene selectivity and improved catalyst durability, as will be discussed further.[122]

8.1.1.1. Method of co-precipitation. The co-precipitation technique entails the controlled precipitation of metal hydroxides from salt precursors, illustrated in Fig. 14. By adjusting

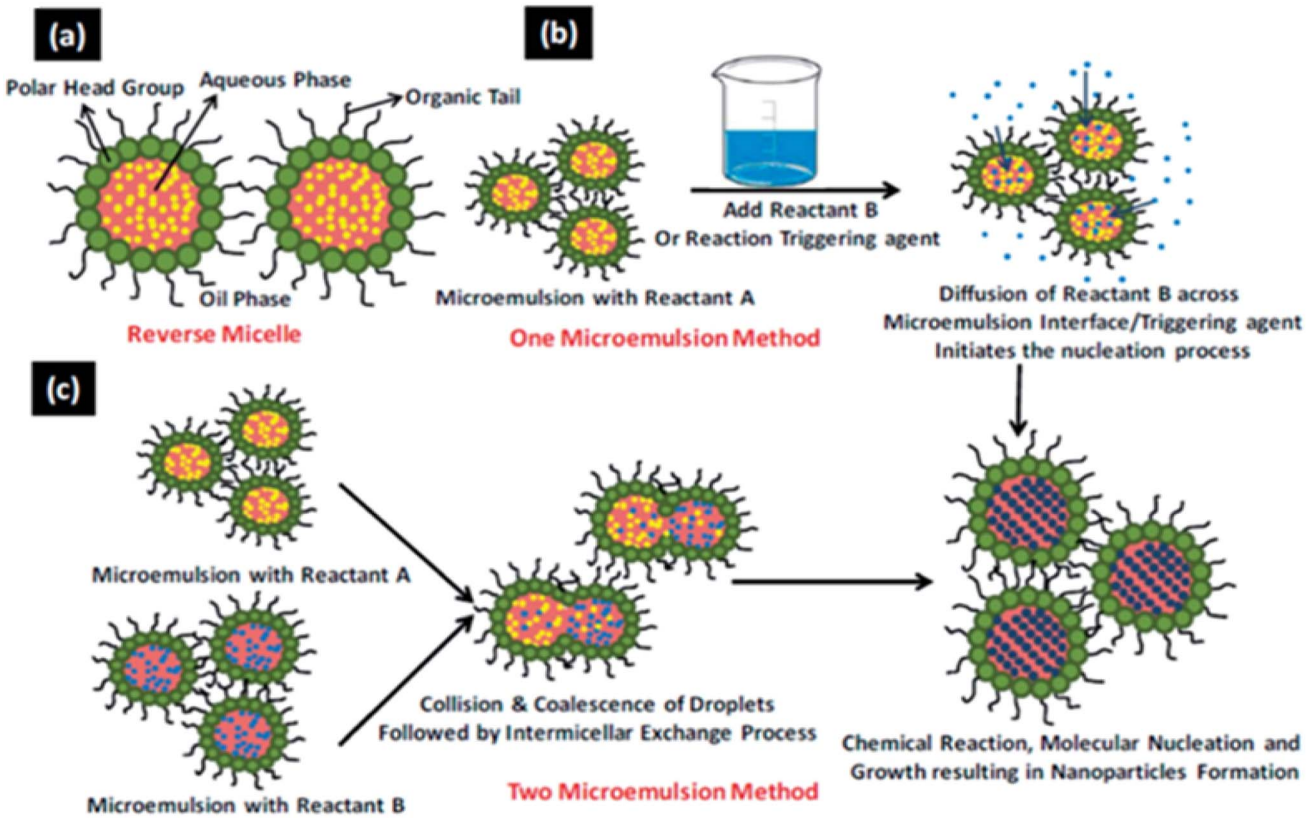

Fig. 15 The overall procedure involves a renowned method of microemulsion. (a) Reverse micellar system (b) one technique of microemulsion and (c) two methods of microemulsion (reprinted with permission,[129] copyright 2015 Royal Society of Chemistry).

parameters like pH, ion concentration, and temperature, researchers can tailor particle size, morphology, and metal dispersion. These adjustments directly influence acidity, porosity, and metal–support interactions, all of which are essential for optimizing ethanol conversion efficiency, ethylene selectivity, and catalyst stability in dehydration reactions.[123,124]

8.1.1.2. Microemulsion technique. The microemulsion technique enables the synthesis of nanoparticles with controlled sizes and uniform structures, which are essential for effective catalyst performance in ethanol dehydration.[126] In this process, metal precursors precipitate as oxo-hydroxides within aqueous droplets, resulting in monodispersed particles. The morphology and dispersion of these particles are influenced by surfactant interactions.[127] Key parameters affecting the reverse micellar system include: (i) the water-to-surfactant molar ratio (Wx), (ii) the intermuscular exchange rate, (iii) the nature of the organic solvent, (iv) the characteristics of the surfactant and co-surfactant, and (v) packaging parameters.[128] These factors directly impact acidity, porosity, and catalytic activity, which in turn affect ethanol conversion and ethylene selectivity. Fig. 15 illustrates the microemulsion approach for preparing nanoparticles specifically designed for ethanol dehydration catalysts.[129]

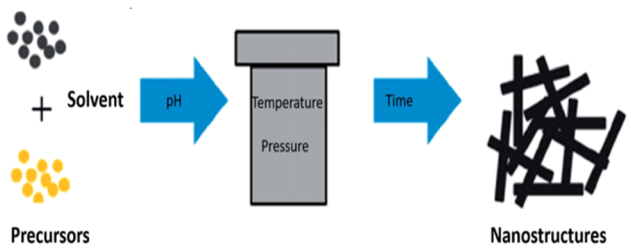

Fig. 16 Hydrothermal synthesis schematic for ethanol dehydration catalysts (reprinted with permission,[126] copyright 2018 Royal Society of Chemistry).

8.1.1.3. Hydrothermal (solvothermal) technique. The hydrothermal or solvothermal technique involves treating metal precursors in a sealed autoclave under high pressure and temperature, often using surfactants to manage particle growth and prevent agglomeration.[130–132] This method facilitates the formation of well-crystallized, multi-element oxide nanoparticles with controlled size, morphology, and surface properties, which are essential for optimizing ethanol conversion efficiency, ethylene selectivity, and catalyst stability in dehydration reactions.[115] Fig. 16 depicts the general hydrothermal synthesis process employed to prepare catalysts specifically designed for ethanol-to-ethylene conversion.[126]

8.1.1.4. Sol–gel method. The sol–gel method allows for the preparation of metal oxide catalysts with controlled porosity, particle size, and surface properties, all of which are crucial for achieving high ethanol conversion and ethylene selectivity.[133] In the alkoxide route, metal alkoxides undergo hydrolysis and condensation in alcoholic solutions to create a porous gel network. Alternatively, the non-alkoxide route employs inorganic salts, such as metal chlorides, which necessitates careful removal of anions to yield pure oxides.[125] Fig. 17 illustrates the sol–gel process for preparing nanomaterials specifically designed for ethanol-to-ethylene catalysts.[115]

8.1.1.5. Microwave irradiation method. The microwave irradiation (MWI) technique is employed to synthesize mesoporous catalysts that exhibit enhanced crystallinity and well-controlled particle sizes ranging from 1 to 5 nm, which are essential for improving ethanol conversion efficiency and ethylene selectivity.[134,135] By directly heating the precursor molecules, microwaves provide faster and more uniform heating compared to traditional methods.[136] This results in improved metal dispersion, increased surface area, and greater accessibility of active sites, all of which are vital for effective ethanol dehydration.[137,138] Fig. 18 illustrates the MWI synthesis process for nanoparticles utilized in ethanol-to-ethylene catalysts. Microwaves generate heat directly within the molecules of the

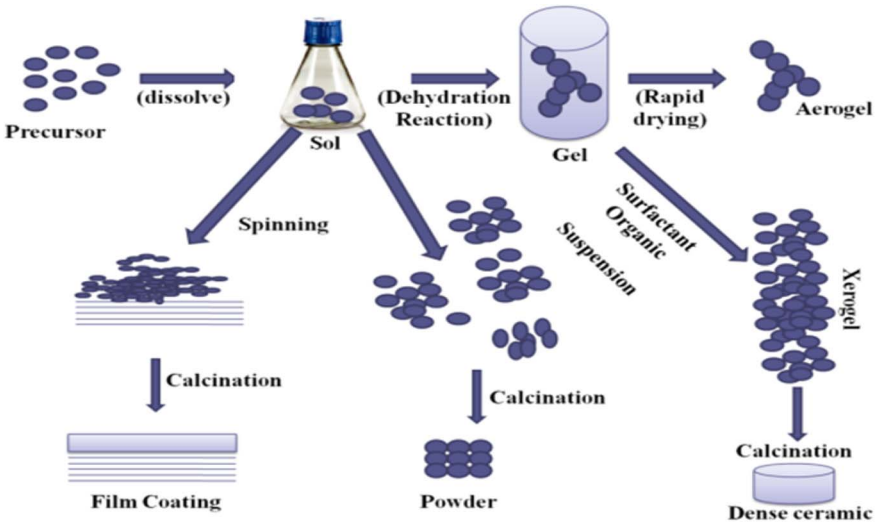

Fig. 17 Sol–gel synthesis schematic for ethanol dehydration catalysts[115] (DOI: https://doi.org/10.1063/1.4915472, Open-source: AIP Conference Proceedings).

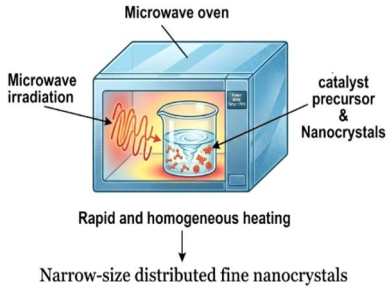

Fig. 18 Microwave irradiation schematic for ethanol dehydration catalysts. Adapted from ref. 139.

material being heated, with electromagnetic fields divided into electrical and magnetic components that interact with materials through various mechanisms.[138]

8.1.1.6. Sonication method. Sonication is a highly effective technique for producing catalysts that possess unique structural properties, small particle sizes, and high purity.[140,141] It works by generating ultrasonic waves in a liquid, which create bubbles that grow and collapse.[142] This process breaks chemical bonds and facilitates the formation of nanoparticles with increased surface area, acidity, and active site exposure.[143] As a result, these characteristics significantly enhance ethanol conversion and ethylene selectivity.[142] Fig. 19 illustrates the sonication mechanism used to prepare ethanol dehydration catalysts.

Table 1 provides a critical comparison of synthesis strategies by correlating preparation methods with their structural effects, catalytic behavior in ethanol dehydration, and practical limitations.

8.1.2. Role of catalyst carriers and metal–support interaction. The catalytic activity of supported catalysts during the dehydration of ethanol is significantly influenced by the physical and chemical characteristics of the support and its interaction with the active metal phase.[145] Beyond providing surface area, the catalyst support affects properties such as metal dispersion, electronic structure, acid site distribution, and resistance to deactivation.[146] Stronger metal–support interactions (MSI) enhance the stability of the active site, modify the strength of Lewis acid sites, and influence ethanol adsorption strength, all of which impact the selectivity between ethylene and diethyl ether.[147] Acidic supports, such as γ-Al_2O_3 and zeolites, with abundant Lewis and Brønsted acid sites, enhance the dehydration process through their multiple acidic sites.[148] In contrast, neutral supports like silicones (SiO_2) facilitate dispersion but do not increase the overall acidity of the catalyst.[149] Reducible oxides, such as TiO_2 and ZrO_2, can alter electronic characteristics and the concentration of oxygen vacancies, affecting the stability of intermediates and resistance to coking.[150] Additionally, porous structures and high surface areas improve mass transfer and reduce concentration gradients, which are essential for achieving high ethylene selectivity on an industrial scale. Thus, optimizing the carrier composition and metal–support interaction is crucial for maximizing activity, selectivity, and long-term stability.[151,152] Table 2 offers a comparative overview that correlates carrier properties with the effects of metal–support interactions and their catalytic consequences in ethanol dehydration.

8.1.2.1. γ-Al_2O_3 catalysts: properties, modifications, and performance. γ-Al_2O_3, commonly known as alumina, is a heterogeneous Lewis acid catalyst known for its high chemical and thermal stability, large surface area, and favorable mechanical properties.[153,154] These characteristics make it a popular choice for ethanol dehydration, which produces ethylene.[155,156] The alumina catalyst derived from sodium aluminate exhibits only weak acid sites, whereas the alumina synthesized from aluminum isopropoxide possesses strong acid sites.[157–159] However, the hydrophilic surface of alumina can become saturated with water, which occupies active sites and diminishes catalytic activity. Additionally, the relatively high reaction temperature (approximately 450 °C) can lead to coke formation, accelerating catalyst deactivation.[155,156]

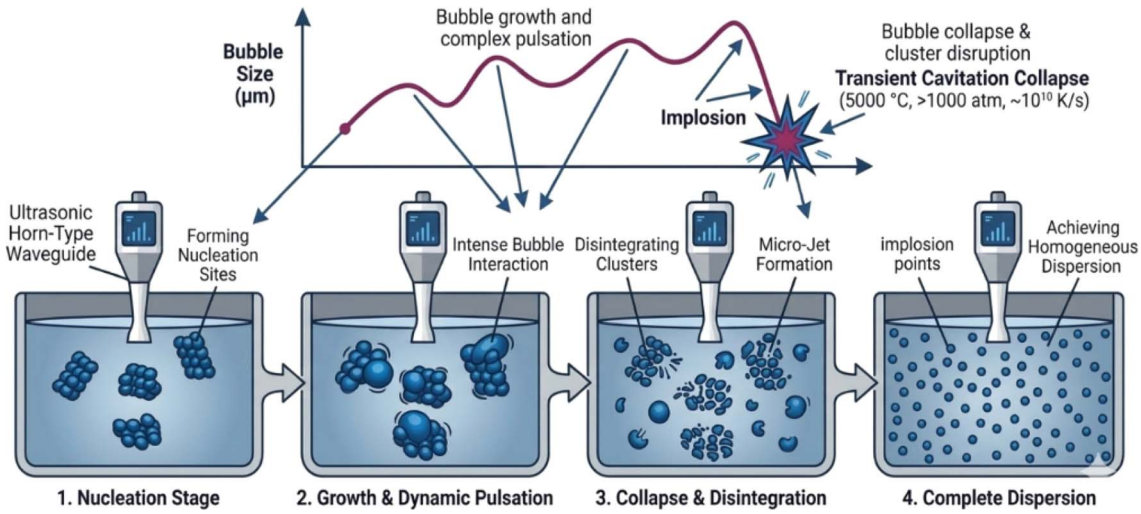

Fig. 19 Sonication schematic for ethanol dehydration catalysts. Adapted from ref. 144.

Table 1 Influence of preparation methods on catalyst properties and ethanol dehydration performance

Preparation method	Structural effect	Catalytic consequence in ethanol dehydration	Main limitation
Co-precipitation	Moderate surface area with relatively uniform metal distribution and limited pore control	Balanced Lewis acidity enables good ethylene formation at high temperatures, though stability is moderate	Potential limitations in pore diffusion may lead to coke formation at high weight hourly space velocities (WHSV)
Sol–gel	High homogeneity, tunable composition, and improved surface area	Enhanced accessibility of acid sites, improved selectivity for ethylene, and better dispersion of active phases	Risk of pore collapse during drying and calcination, along with complexities in scaling up
Hydrothermal/ solvothermal	High crystallinity, well-defined pore structure, and enhanced framework stability	Improved diffusion and hydrothermal stability, enhanced catalyst lifetime, and stable selectivity	Increased synthesis costs and extended preparation time
Microemulsion	Small particle size with a narrow size distribution	Increased exposure of active sites may allow for lower reaction temperatures	Limited scalability and difficulties in achieving reproducibility
Microwave-assisted	Rapid nucleation resulting in small crystallites and improved dispersion	Faster synthesis and enhanced catalytic activity resulting from smaller particle sizes	Equipment costs and constraints related to scaling up
Sonochemical	Enhanced metal–support interaction; surface defect formation	Modified Lewis acidity with tunable selectivity for ethylene and DEE	Challenges in industrial implementation

Table 2 Effect of catalyst carriers on ethanol dehydration performance

Carrier	Key properties	Metal–Support interaction effect	Catalytic performance characteristics	Main limitation
γ-Al_2O_3	Moderate to high surface area; strong Lewis acidity	Enhances metal dispersion; provides intrinsic acid sites	High conversion; good ethylene selectivity at elevated temperatures	Coke formation during prolonged operation
SiO_2	High surface area; weak acidity	Improves metal dispersion without significant electronic modification	Stable but exhibits lower intrinsic dehydration activity	Limited acidity; may require promoters
Zeolites (HZSM-5)	Strong Brønsted acidity; microporous structure	Confinement effect enhances adsorption and selectivity	Very high ethylene selectivity; tunable acidity	Diffusion limitations; prone to coke formation
TiO_2	Reducible oxide; oxygen vacancies	Alters electronic structure; improves metal–support interaction	Enhanced stability; moderate control over selectivity	Lower intrinsic acidity
ZrO_2	Amphoteric character; thermal stability	Modifies acid–base balance; enhances coke resistance	Improved durability; tunable selectivity	Moderate activity without modification
Composite oxides	Adjustable acidity and porosity	Synergistic tuning of metal–support interaction and acid sites	Enhanced activity and stability	Synthesis complexity

To address these challenges, recent studies have focused on modifying γ-Al_2O_3 to improve its activity and selectivity while lowering operational temperatures. Various modifications have been explored, including metal loadings such as TiO_2,[160] Ni, and CaO,[161] as well as phosphorus modification (H_3PO_4) and the addition of noble metals like Pd. For instance, the incorporation of 0.5 wt% Pd onto phosphorus-modified γ-Al_2O_3 (Pd/Al_2O_3-P, Fig. 20(a)) introduces additional Brønsted acid sites, enhancing ethylene selectivity and reducing coke deposition. This modification achieves high ethanol conversion (99.96%) and ethylene selectivity (99.4%) at 460 °C.[75] In contrast, phosphorus-modified γ-Al_2O_3 without Pd (5P/Al_2O_3, Fig. 20(b)) optimizes weaker surface acidity, making it more suitable for the selective production of diethyl ether (DEE) at moderate temperatures (~300 °C), resulting in approximately 34% DEE yield and 70% selectivity.[76] This analysis underscores the trade-off between product selectivity and catalyst stability: while Pd/Al_2O_3-P is advantageous for ethylene production at high temperatures, 5P/Al_2O_3 is preferable for DEE synthesis at lower temperatures. Overall, these comparisons illustrate that tuning γ-Al_2O_3 through metal loading or phosphorus modification enables selective control over ethanol dehydration products by adjusting acidity, metal–support interactions, and porosity, thus providing flexibility based on the desired industrial outcome.[162,163]

8.1.3. Zeolites for ethanol dehydration. Zeolites are hydrated microporous aluminosilicates consisting of interconnected aluminum (AlO_4) and silica (SiO_4) tetrahedra. This structure forms three-dimensional frameworks with molecular-sized channels measuring 0.3 to 1.5 nm.[164,165] Their uniform pore systems, high surface area, strong Brønsted and Lewis acidity, and excellent hydrothermal stability make zeolites highly effective solid-acid catalysts for ethanol dehydration.[166] They exist in various crystalline structures characterized by

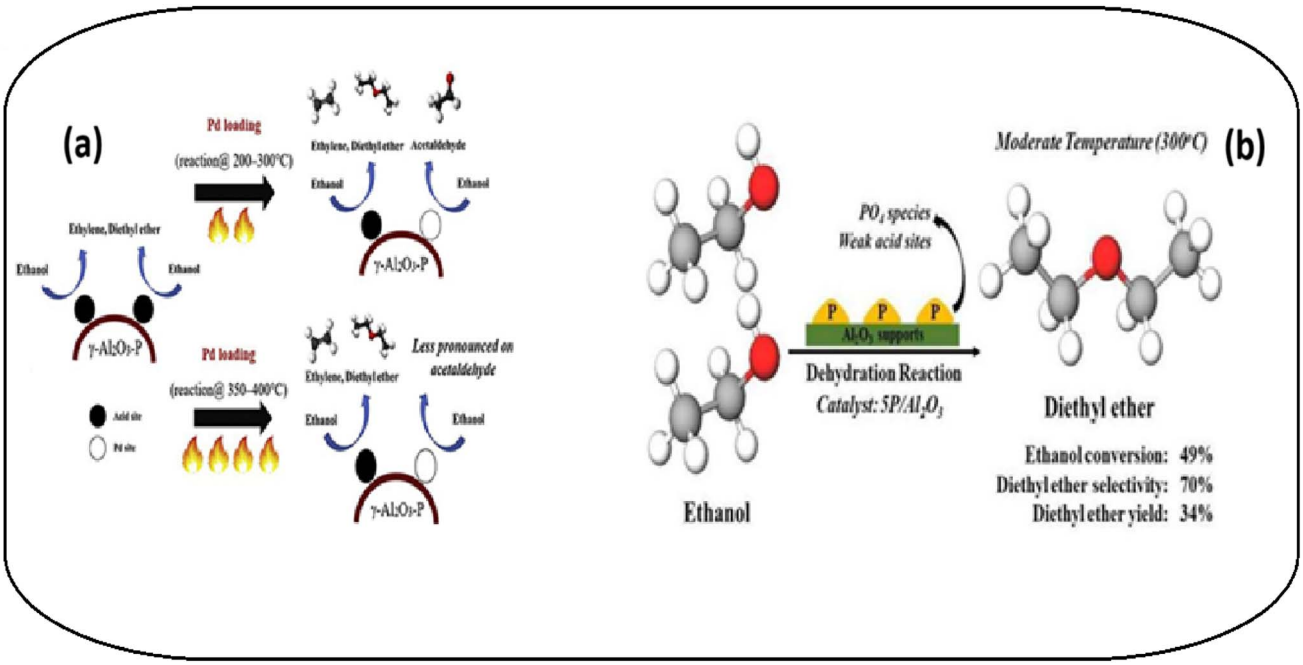

Fig. 20 γ-Al_2O_3 modification for ethanol dehydration. (a) 0.5 Pd/Al_2O_3-P for ethylene production, (b) 5P/Al_2O_3 for diethyl ether production[76] (reprinted with permission,[75] copyright 2021 Elsevier), (b) (DOI: https://doi.org/10.9767/bcrec.14.1.2436.1-8, Open-source publisher: BCREC Group).

large, regularly arranged open pores that are comparable in size to small molecules. Notable examples include zeolite A,[167] zeolite X,[167] zeolite Y (used as a catalyst for catalytic cracking),[168] and ZSM-5.[51]

Among zeolite catalysts, HZSM-5 is regarded as one of the most promising options for industrial ethanol dehydration. It operates efficiently at temperatures below 300 °C, achieving ethanol conversion rates of up to 98% with approximately 95% selectivity for ethylene at 300 °C.[169] A significant advantage of zeolites over alumina is their capability to process diluted ethanol feeds, which reduces the need for expensive water dehydration.[170] However, the inherent microporous structure of conventional ZSM-5 can restrict mass transfer and limit access to active sites, resulting in diffusion constraints and potential catalyst deactivation. To address these challenges, recent research has focused on structural and compositional engineering. Alkaline treatment has been employed to introduce mesoporosity, which enhances surface area and reactant diffusion. This modification allows for operation at lower temperatures, yielding improved ethylene selectivity (up to 99.8%) and better resistance to coking.[171]

Overall, recent advances in zeolite-based catalysts can be grouped into three main strategies: (1) generating hierarchical pores to enhance mass transport, (2) incorporating metals to modify acid–metal interactions and improve low-temperature activity, and (3) forming composite acid phases to increase strong acidity and catalytic stability.[172,173]

These strategies signify a shift from merely controlling acidity to designing multifunctional catalysts that integrate optimized porosity, enhanced active-site accessibility, and improved durability.[174] The performance improvements documented in various studies align with these three approaches: hierarchical pore generation, metal incorporation, and composite acid-phase formation.[175] Table 3 provides a comparative overview of modified zeolite catalysts, highlighting the relationship between framework engineering, modification strategies, and their catalytic performance in ethanol dehydration.

8.1.4. Silica–alumina. Amorphous silica–alumina (aluminosilicate) catalysts are commonly used for ethanol dehydration due to their strong Brønsted and Lewis acid sites.[180] The Brønsted sites can reversibly convert to Lewis sites when dehydrated at elevated temperatures, which directly impacts catalytic performance. The high density of strong acid sites in silica–alumina typically favors the conversion of ethanol to ethylene over diethyl ether (DEE). Therefore, controlling the strength and distribution of acid sites is essential for tuning selectivity.[181,182]

Several strategies have been employed to regulate acidity, including the selective poisoning of strong acid sites with weak bases and modifying the Al/Si molar ratio.[183] The Al/Si ratio significantly influences acid density, acid strength, and catalytic stability.[167] While strong acidity promotes ethylene production, excessive acid strength can lead to side reactions and coke formation. Thus, achieving an optimized acid balance is crucial for stable and selective ethanol dehydration.[168]

8.1.4.1. Mesoporous silica materials. To address the diffusion limitations seen in conventional amorphous silica–alumina, researchers developed mesoporous silica materials.[184] Notable families such as MCM (Mobil Composition of Matter), SBA (Santa Barbara Amorphous), and KIT (Korean Advanced

Table 3 Comparative performance of zeolite catalysts in ethanol dehydration

Catalyst type	Modification strategy	Temperature (°C)	Ethanol conversion (%)	Ethylene selectivity (%)	Reference
Hierarchical MFI (Si/Al = 40)	Ultrasonic desilication (mesopore formation)	210 270–290	40–68 100	DEE ≥ 95	176
Cu-SSZ-13	Metal incorporation (Cu complex)	212	~100	>99	64
Dealuminated ZSM-5	Acid density optimization	220	98.5	100	51
IM-5	Topology engineering	260	100	Highest DEE Ethylene yield balance	171
TNU-9	Topology variation	260	100	Selective to ethylene + C_3^+	171
Ti-deZSM-5	Metal-doped framework	280	96	88	177
Rho zeolite	High surface area framework	250–350	100	>98	178
Zeolite β/AgPW	Composite acid phase	—	81–86	High	179

Institute of Science and Technology) have gained significant attention due to their highly ordered mesostructures.[185] These materials offer large surface areas (over 900 $m^2 g^{-1}$ in some cases), tunable pore diameters (ranging from 2 to 30 nm), and narrow pore size distributions with a well-defined hexagonal layout.[186] These structural features increase the accessibility of ethanol molecules to active sites, thereby enhancing catalytic efficiency in dehydration reactions.

In 1992, scientists at Mobil Corporation discovered a new class of silicate materials known as the M41S phase, which features ordered mesoporosity, tunable pore diameters (2–30 nm), and high specific surface areas (greater than 900 $m^2 g^{-1}$), as illustrated in Fig. 21. The most well-known members of this class include MCM-41 (characterized by hexagonal mesopores),[187] MCM-48 (with a cubic mesopore design), and MCM-50 (featuring a lamellar structure).[188]

8.1.4.2. MCM-41. MCM-41 is part of the M41S family and features a one-dimensional hexagonally arranged cylindrical mesopore system. It has a high surface area and large pore volume, with pore diameters that can be adjusted independently. The pores are larger than those found in zeolites, allowing for easier porosity exchange.[189,190] The large one-dimensional pores facilitate the easier diffusion of reactants to active sites, thereby increasing reaction rates.

The synthesis of MCM-41 involves surfactants that form micelles in the synthesis solution. These micelles serve as templates, facilitating the creation of the mesoporous framework.[191] Typically, surfactants such as cetyltrimethylammonium bromide (CTAB) are used, which form rod-like micelles that act as templates for silica condensation.[192,193] Following calcination, the organic template is removed, resulting in uniform mesopores. Fig. 22 illustrates the formation mechanism of the M41S mesostructure, where surfactant micelles arrange into a hexagonal array and are subsequently coated with silica species before template removal.[190,194] Microwave-assisted synthesis enhances pore uniformity, which helps ensure consistent catalytic performance. Additionally, post-synthetic modifications, like the introduction of Brønsted acid sites or metal incorporation, further enhance catalytic selectivity and activity.

MCM-41 is characterized by a high surface area, large pore volume, and tunable pore diameter. Its larger pores significantly enhance reactant diffusion and accessibility to active sites when compared to zeolites. However, the one-dimensional pore structure may still create diffusion limitations under high space velocity conditions.[195] Additionally, microwave-assisted synthesis improves homogeneity and increases the nucleation rate, leading to better structural control.[196]

8.1.4.3. SBA-15. Santa Barbara Amorphous mesoporous (SBA) material was synthesized in 1998, featuring a hexagonal array of pores.[197] Its well-defined pore structure, inert framework, thick walls, and excellent thermal and hydrothermal

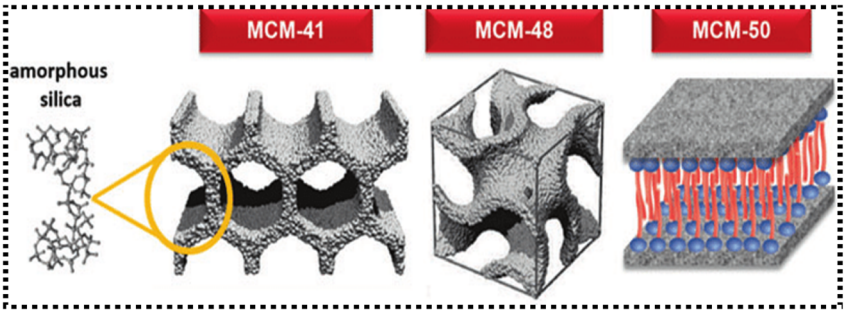

Fig. 21 Schematic of the phase structure of M41S mesoporous materials[188] (DOI: https://doi.org/10.1007/978-3-319-48281-1_43-1, Open-source: Springer Nature).

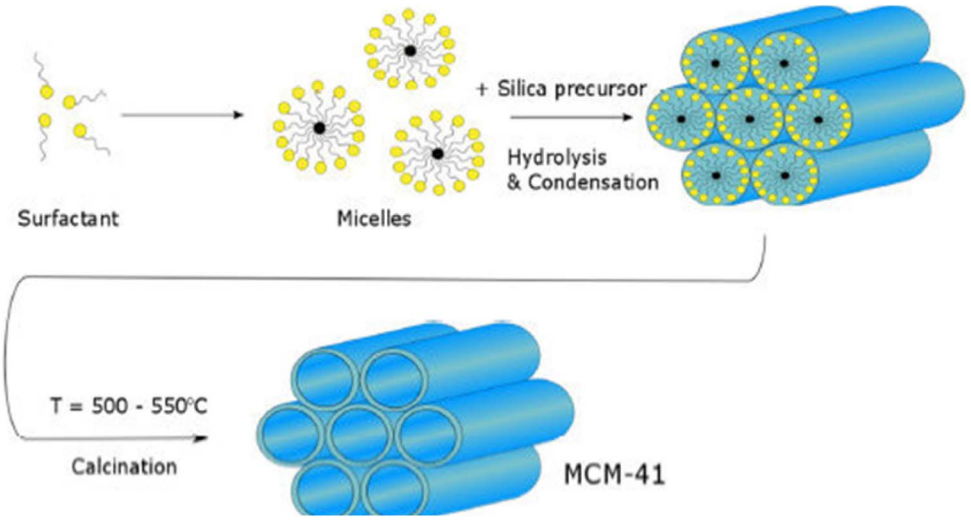

Fig. 22 Schematic illustration of the micelle-templated formation mechanism of hexagonal MCM-41 mesostructured.[196] (DOI: https://doi.org/10.22153/kej.2019.11.003, Open source: Al-Khwarizmi College of Engineering).

stability have attracted significant interest from researchers. SBA-15 boasts several appealing characteristics, including a large surface area (600–1000 m^2 g^{-1}),[197] two-dimensional molecular sieves with *P6mm* hexagonal symmetry, and thick walls measuring 3–6 nm.[198] The thick walls improve thermal and hydrothermal stability, which is crucial for the dehydration of ethanol at high temperatures. The synthesis process employs Pluronic triblock copolymers (PEO–PPO–PEO) as structure-directing agents under strongly acidic conditions, along with tetraethyl orthosilicate (TEOS) as the silica source.[199–202] The formation of micelles occurs due to the orientation of hydrophilic groups towards the outside and hydrophobic groups within the micelles. The interactions between water molecules and alkylene oxides create hydrogen bonds, illustrating the SBA-15 synthesis mechanism shown in Fig. 23.

The large surface area facilitates efficient access of reactants to active sites, enhancing catalytic performance. Due to the weak intrinsic acidity of pristine SBA-15, the post-synthetic incorporation of aluminum or metal species creates Brønsted acid sites or bifunctional centers, which significantly boosts catalytic efficiency and selectivity.

This structural difference is crucial for its catalytic behavior. Compared to MCM-41, the thicker pore walls of SBA-15 enhance its structural stability under reaction conditions, particularly during ethanol dehydration at elevated temperatures.[203] However, like pure silica MCM-41, pristine SBA-15 exhibits weak intrinsic acidity. Consequently, its catalytic performance heavily relies on post-synthetic modifications, such as aluminum incorporation to generate Brønsted acid sites or metal loading to introduce bifunctional activity.[204]

8.1.4.4. Aluminum-incorporated MCM-41 and SBA-15. Pure mesoporous silica does not possess sufficient intrinsic acidity for effective ethanol dehydration. To address this, incorporating aluminum into MCM-41 or SBA-15 frameworks introduces both Brønsted and Lewis acid sites while enhancing hydrothermal stability.[205,206]

Aluminum incorporation can be achieved through two primary methods:

• Direct (one-pot) synthesis, where aluminum precursors are added during the formation of the mesostructure, ensuring strong metal–support interactions.[207]

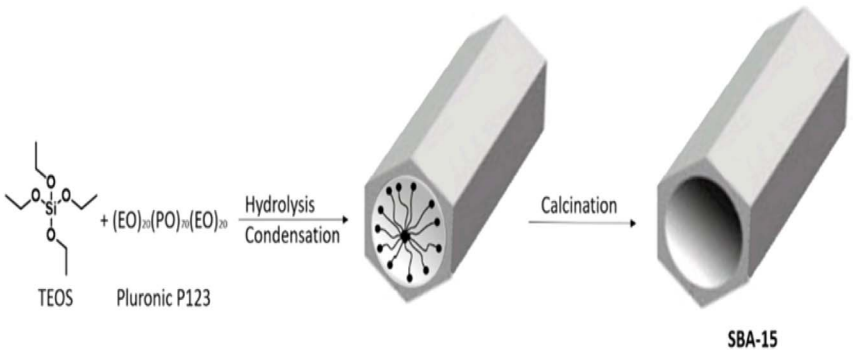

Fig. 23 Schematic representation of the synthesis procedure for SBA-15.[204] (DOI: https://doi.org/10.3390/catal9120984, Open-source: MDPI).

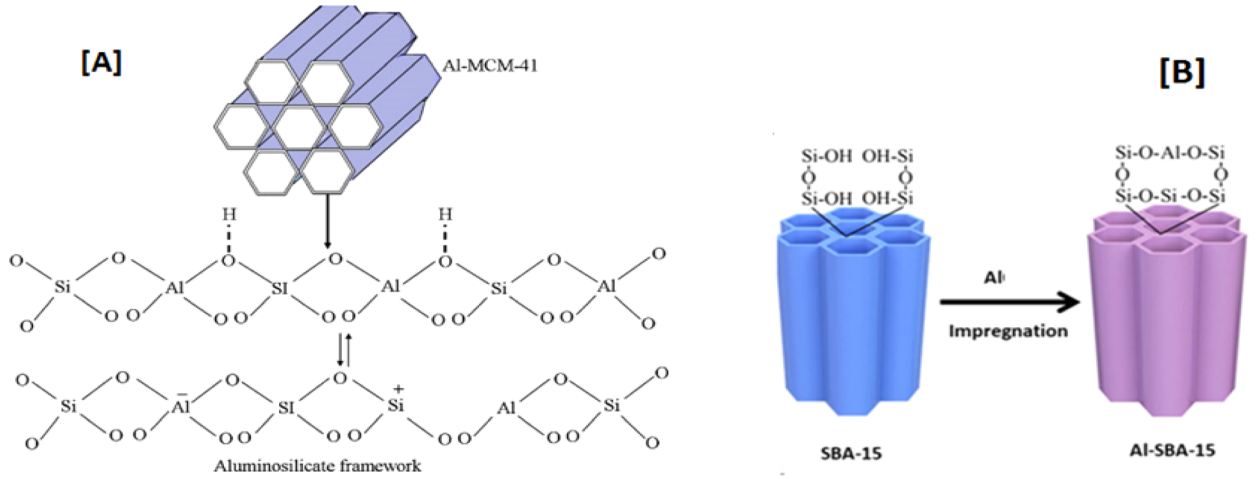

Fig. 24 Wall structure of Al-incorporated MCM-41 (A) and SBA-15 (B) materials (reprinted with permission,[211] copyright 2010 Elsevier).

• Post-synthesis methods, such as incipient wetness impregnation or wet impregnation, which allow for controlled loading of aluminum species.[208]

Fig. 24 depicts the wall structure of Al-incorporated MCM-41 and SBA-15 materials.[209] The figure demonstrates that aluminum species are integrated within the silica framework rather than simply deposited on the external surface, resulting in the formation of framework-associated Brønsted and Lewis acid sites. Direct (one-pot) synthesis typically ensures better structural integration and a homogeneous distribution of aluminum within the mesoporous walls, while post-synthesis techniques offer greater flexibility in adjusting acid density and surface composition. However, aluminum incorporation may slightly alter pore diameter and surface area due to partial framework distortion.[210]

Silica–alumina-based catalysts exhibit catalytic behavior that is heavily influenced by their acidity and structural properties. Specifically, alumina–silica composites with optimized aluminum content show enhanced performance in dehydration. As shown in Fig. 25, the dehydration pathway for ethanol and bioethanol over the Al–SSP catalyst occurs through acid-site activation, primarily resulting in ethylene formation at higher temperatures. The catalyst's performance is significantly affected by the type of acidity, porosity, and preparation method.[212]

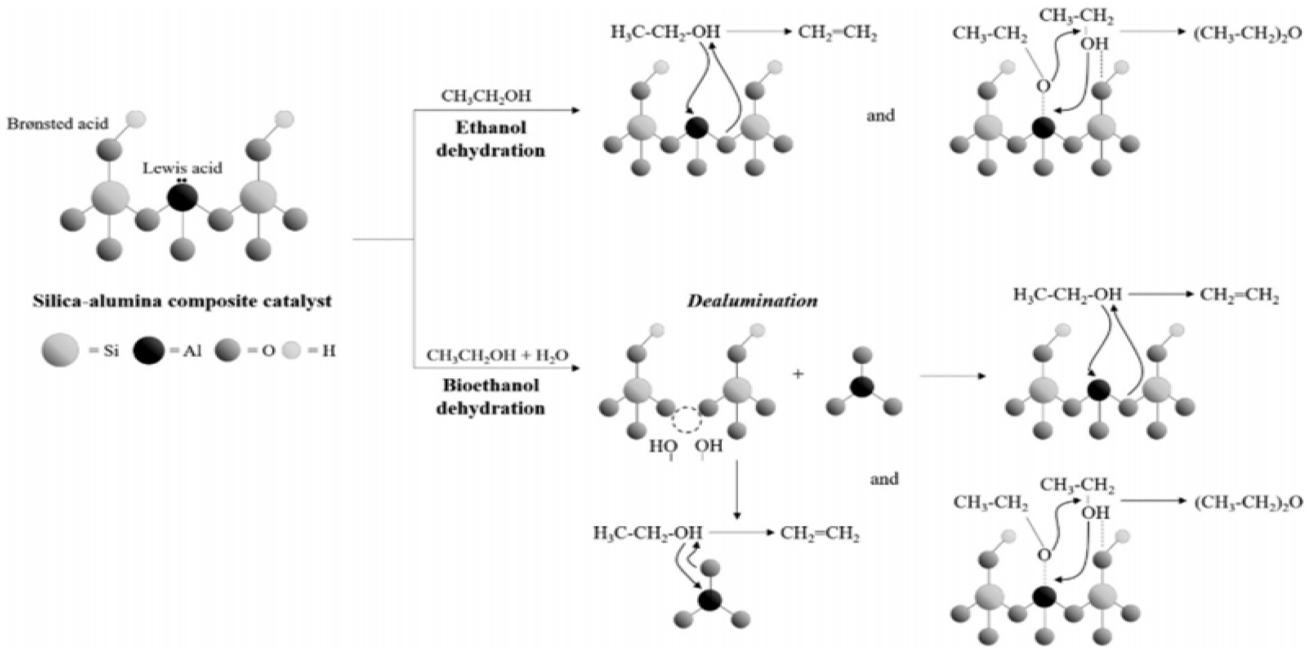

Fig. 25 Reaction scheme for ethanol and bioethanol dehydration over alumina–silica composite (Al–SSP) catalyst (reprinted with permission,[212] copyright 2020 Elsevier).

Table 4 Comparative analysis of silica–alumina-based catalysts for ethanol dehydration

	Preparation/method	Ethanol conversion (%)	Ethylene selectivity (%)	DEE selectivity (%)	Reference
NHSG mesoporous organosilica	Non-hydrolytic sol–gel with Al, Nb, or Sn	64.7–95.5	64.7–95.5	2–18	209
Commercial silica–alumina	Conventional preparation	100	96–100	~30	213
Zeolites (HZSM-5, MFI, *etc.*)	Dealumination, desilication, metal/La/P impregnation catalyst type	91–100	88–100	Low	214
Alumina-silica composite (Al-SSP)	Sol–gel, varying Al content (20–80 mol%)	98	99	Low	212

The 60Al-SSP sample shows the highest acidity, resulting in 98% ethanol conversion and 99% ethylene selectivity at 400 °C, with good stability over 10 h of operation. Compared to NHSG-prepared mesoporous catalysts and conventional silica–alumina, the Al–SSP system offers a favorable balance between acid strength, conversion efficiency, and operational stability, although slight deactivation due to coke formation may occur during prolonged bioethanol dehydration. The comparative analysis in Table 4 summarizes the relative strengths, weaknesses, and industrial potential of these catalysts.

The comparative analysis of alumina–silica catalysts clearly shows their effectiveness in dehydrating ethanol to produce ethylene. This process underscores the importance of acid site density, strength, and distribution in influencing catalytic performance.[215]

While dehydration is the primary method for valorizing bioethanol, ethanol can also undergo additional transformations beyond merely removing water. When using multifunctional catalysts with a balanced mix of acidic, basic, and/or metallic sites, ethanol-derived intermediates like ethylene or acetaldehyde can engage in C–C bond-forming reactions, such as oligomerization, aldol condensation, metathesis, and Guerbet coupling[216] These sequential upgrading pathways broaden the range of products to include higher hydrocarbons and oxygenates, such as propylene, 1,3-butadiene, and higher alcohols, thus enhancing the potential for sustainable catalytic conversion of ethanol for petrochemical applications.[217]

9. Beyond dehydration: ethanol upgrading *via* C–C coupling reactions

Ethanol upgrading through C–C bond formation occurs through several key pathways, including the conversion to propylene, 1,3-butadiene, and higher alcohols.[218] These processes involve tandem catalytic sequences that integrate dehydration with dehydrogenation, condensation, and hydrogen-transfer reactions using multifunctional catalysts.[219] Unlike simple dehydration, these upgrading routes necessitate a careful balance of acidic, basic, and metallic active sites, making catalyst design a crucial factor that influences activity, selectivity, and stability.[220]

9.1. Ethanol to propylene

The ethanol-to-propylene (ETP) process follows integrated dehydration–coupling pathways rather than a single elementary reaction.[221] Initially, ethanol is dehydrated over acidic sites to produce ethylene. This ethylene then undergoes oligomerization, isomerization, and metathesis reactions with the help of bifunctional catalysts to yield propylene.[222,223] The efficiency of this cascade process heavily relies on the strength and distribution of acid sites, along with the presence of metallic or shape-selective functions that facilitate controlled C–C bond formation and minimize coke formation.[224]

Propylene is one of the most widely produced petrochemicals after ethylene and has extensive applications in the synthesis of polypropylene, acrylonitrile, acrylic acid, acrolein, propylene oxide, glycols, oxo alcohols, cumene, isopropyl alcohol, and acetone.[225] Global propylene consumption exceeds 100 million tons and is projected to reach 135 million tons by 2025, with an annual growth rate of approximately 4%.[226] Traditionally, propylene is obtained from non-renewable fossil resources, primarily through steam cracking of light naphtha at high temperatures (750–850 °C) and very short residence times (0.08–0.25 s), or through fluid catalytic cracking using Y-zeolite catalysts derived from natural gas and coal.[227]

Ethanol conversion to propylene encompasses a series of reactions, including dehydration, dehydrogenation, and C–C bond formation, which go beyond mere ethanol dehydration.

The general reaction sequence includes:

(1) Ethanol dehydration to ethylene:

Ethanol is first dehydrated to ethylene as described in eqn (1).

(2) Ethylene dimerization and rearrangement to higher hydrocarbons:

$$2CH_2{=}CH_2 \rightarrow CH_2{=}CHCH_2CH_3 \rightarrow CH_3CH{=}CHCH_3 \quad (4)$$

$$CH_3CH{=}CHCH_3 + CH_2{=}CH_2 \rightarrow 2CH_2{=}CHCH_3 \quad (5)$$

A mechanistic proposal suggests that ethylene is activated over ZSM-5 zeolite, resulting in the formation of a carbene species through π-complexation. This species then reacts with ethylene to produce propylene:[228]

$$C_2H_4 \rightarrow (CH_2) \quad (6)$$

$$CH_2 + C_2H_4 \rightarrow C_3H_6 \quad (7)$$

The confinement effect in ZSM-5 micropores is essential for stabilizing carbene intermediates and promoting selective propylene formation, highlighting the significance of pore architecture in catalytic performance.[229]

Iwamoto *et al.*,[225] reported a one-step conversion of ethanol to propylene using nickel ion-loaded mesoporous silica at 400 °C. This process achieved 68% ethanol conversion and 48% selectivity for propylene. The reaction mechanism involves the dimerization of ethylene to form 1-butene, followed by isomerization to 2-butene, and then metathesis with ethylene to produce propylene, as illustrated in Fig. 26. Additionally, diethyl ether (DEE) is formed as a side product at 250 °C, which can revert to ethanol and ethylene. At higher temperatures (300–400 °C), ethylene and butane intermediates are efficiently converted to propylene. These results demonstrate that metal–support interactions in mesoporous silica greatly affect propylene selectivity by adjusting the balance between oligomerization and metathesis pathways.[230]

9.2. Ethanol to 1,3-butadiene

1,3-Butadiene is a crucial bulk chemical in the petrochemical industry, primarily used in the production of synthetic rubber (such as styrene–butadiene rubber and polybutadiene) and other applications, including chloroprene, nitrile rubber, acrylonitrile, elastomers, and resin.[231–233] Global production was approximately 10 million metric tons in 2012, with projections indicating growth to 15 million tons by 2023.[234] Industrially, butadiene is obtained either from naphtha steam cracker fractions or through catalytic or oxidative dehydrogenation of *n*-butane and *n*-butene.[233,235] Projections indicate that butadiene consumption may increase from approximately 526 thousand tons in 2010 to over 1.2 million tons by 2030.[219]

Ethanol can be converted to 1,3-butadiene through tandem catalytic pathways involving sequential dehydrogenation, aldol condensation, and dehydration reactions.[236] This transformation is especially sensitive to the catalyst's acid–base balance. Excessive acidity promotes unwanted dehydration to ethylene, while insufficient redox functionality restricts the formation of acetaldehyde.[232]

The choice of catalysts significantly impacts the rate, selectivity, and yield. Zirconium-based catalysts, along with various metal oxides (such as MgO/SiO_2, TiO_2, Al_2O_3, Nb_2O_5, ZrO_2) and metals (including Ag, Cu, Ni) supported on mesoporous silica, have been extensively studied.[237,238] For example, $Ag–ZrO_2/SiO_2$ demonstrated 88% ethanol conversion with 73.9% selectivity to 1,3-butadiene at 320 °C, 73.9% selectivity dehydration.[236] The high selectivity observed is due to the synergistic interaction between the dispersed ZrO_2 acid–base sites and the metallic Ag centers. This interaction facilitates hydrogen-transfer steps and minimizes side reactions.[239]

The transformation of ethanol to butadiene generally follows five key steps, as shown in Fig. 27: (i) the conversion of ethanol to acetaldehyde; (ii) aldol condensation to form 3-hydroxybutanal; (iii) dehydration to produce crotonaldehyde; (iv) a hydrogen-transfer reaction yielding crotyl alcohol; and (v) the final dehydration to generate 1,3-butadiene.[240]

This multistep mechanism clearly shows that upgrading ethanol necessitates cooperative catalytic functions instead of isolated acidic sites, setting it apart from traditional dehydration chemistry.[241]

This framework highlights that upgrading ethanol to higher hydrocarbons involves more than just simple dehydration; it also includes both acid- and base-catalyzed C–C coupling reactions. These pathways showcase the versatility of modified catalysts in the sustainable valorization of bioethanol.[242]

9.3. Ethanol to higher alcohols (Guerbet reaction)

The upgrading of ethanol to higher alcohols (C_2^+), particularly n-butanol, has become a significant area of research, moving beyond the simple dehydration to ethylene. Higher alcohols offer enhanced fuel properties compared to ethanol and are regarded as promising renewable fuel additives and chemical intermediates. However, developing efficient catalytic systems for selective ethanol coupling remains a challenge.[243]

The conversion process typically follows the Guerbet reaction mechanism, which consists of three main stages:

(i) Dehydrogenation of ethanol to acetaldehyde, (ii) aldol condensation to form β-hydroxy aldehydes, followed by dehydration, and (iii) hydrogenation to produce higher alcohols.[244]

The aldol condensation stage is often the rate-determining step, requiring well-tuned basic or amphoteric surfaces to stabilize enolate intermediates.[245] Unlike direct dehydration, the Guerbet process necessitates multifunctional catalysts that can simultaneously promote both redox and acid–base reactions. Catalyst optimization requires a careful balance between metallic dehydrogenation sites and acid–base centers to enhance C–C coupling while minimizing parallel dehydration to ethylene.[246]

Achieving high selectivity toward C_4^+ alcohols relies on the controlled interplay between these catalytic functions. Ethanol molecules first adsorb onto metal sites (*e.g.*, Ni, Cu, or Ag), where they dehydrogenate into intermediates such as

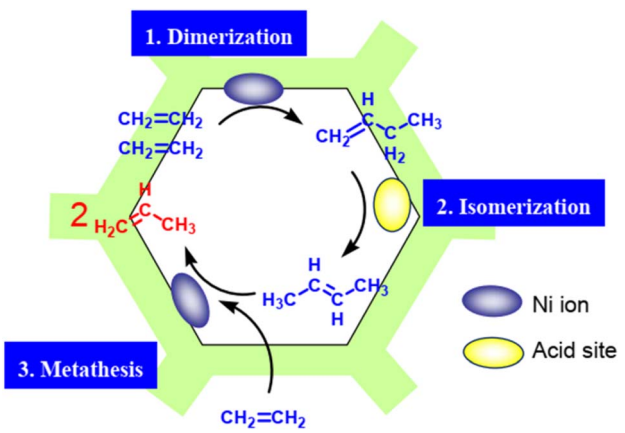

Fig. 26 Proposed reaction mechanism for the conversion of ethylene to propylene on nickel ion-loaded MCM-41.[225] (DOI: https://doi.org/10.3390/molecules16097844, Open-source: MDPI).

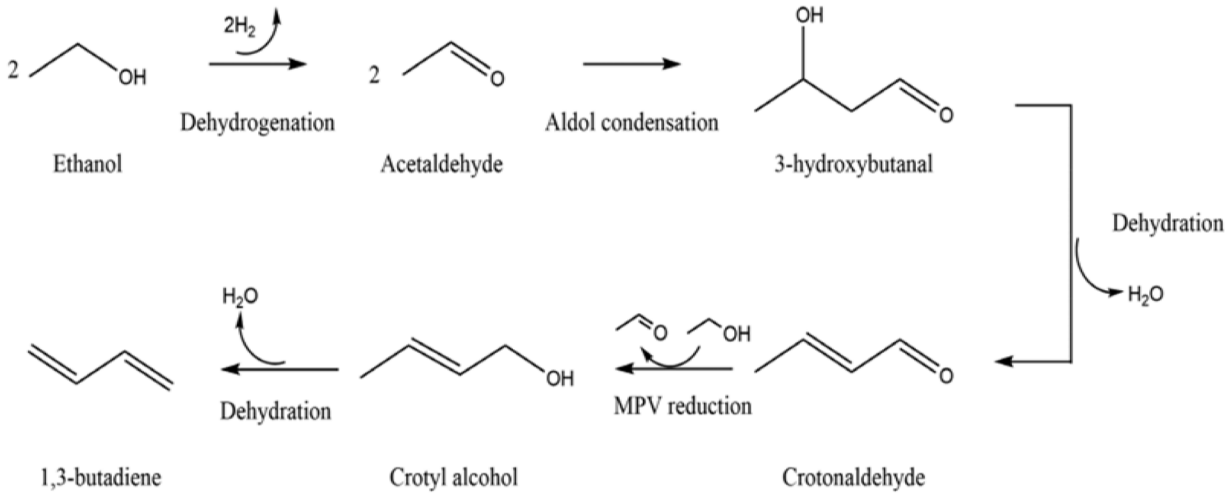

Fig. 27 Reaction mechanism of ethanol conversion to 1,3-butadiene (reprinted with permission,[240] copyright 2012 Elsevier).

$CH_3CH_2O^*$, CH_3CHO^*, CH_3CO^*, and $CH_2CH_2OH^*$. These intermediates are then catalyzed by supports with aldol condensation activity on basic or amphoteric surfaces, leading to the formation of C–C coupled intermediates.[247] These intermediates are subsequently dehydrated and hydrogenated to produce C_4^+ alcohols (*e.g.*, $CH_3CH(OH)CH_2CH_2O^*$).[248] The delicate balance between metallic dehydrogenation sites and acid–base functionalities is crucial for achieving high selectivity toward higher alcohols while minimizing competing dehydration pathways.[249]

Recent advancements underscore the importance of rational catalyst design, which includes optimizing metal–support interactions, tuning acid–base properties, and refining reaction conditions to enhance both activity and stability.[250] This approach illustrates that ethanol valorization goes beyond simple dehydration, integrating C–C coupling strategies made possible by carefully engineered catalytic systems.

These findings confirm that valorizing ethanol through C–C coupling reactions is a sophisticated catalytic strategy. It goes beyond simple dehydration and necessitates careful engineering of both the structure and composition of the catalysts.[251]

10. Conclusion and remarks

The abundance and affordability of bioethanol offer a promising opportunity for its use as a renewable platform molecule in the production of value-added chemicals. Catalytic ethanol dehydration is the most established and primary transformation route, facilitating the sustainable production of ethylene and diethyl ether, which are important petrochemical intermediates. The catalytic dehydration of ethanol serves as a sustainable alternative to traditional petrochemical methods, reducing greenhouse gas emissions and dependence on finite fossil fuels.

This review goes beyond dehydration to critically assess the upgrading of ethanol into higher-value chemicals like propylene and 1,3-butadiene using multifunctional catalytic systems. By comparing catalyst performance, reaction mechanisms, and identifying research gaps, we establish a framework for understanding the current state of the art and guiding future research efforts. Although significant progress has been made in enhancing catalyst performance, stability, and selectivity, challenges persist. These include the need for lower reaction temperatures, longer catalyst lifespans, and more economical integration of ethanol-to-ethylene and ethanol-to-propylene processes. Future research should prioritize the design of catalysts that balance acidity and basicity to optimize product distribution, investigate tandem reaction pathways for higher alcohols and hydrocarbons, and develop scalable, cost–effective processes for upgrading bioethanol. Moreover, incorporating these catalytic processes into existing biorefineries and assessing the economic and environmental impacts of each step will be crucial for the industrial implementation of ethanol valorization technologies.

In summary, although this review does not introduce any new catalysts, it offers a thorough and critical evaluation of existing catalytic systems, insights into their mechanisms, and highlights research gaps. This makes it a valuable resource for researchers and practitioners in the field, underscoring the importance of an analytical perspective in ethanol valorization studies.

Author contributions

Rasha S. Mohamed: conceptualization of the review, investigation, validation, writing – original draft preparation, writing – review and editing, visualization, supervision and resources; Heba M. El Sharkawy: resources, validation, conceptualization, visualization, draft preparation, writing – review and editing. All authors contributed to discussion of the content and have read and agreed to the published version of the manuscript.

Conflicts of interest

The authors confirm this article has no conflicts of interest.

Data availability

This manuscript is a review article and does not report new experimental, computational, or original datasets. All data discussed and presented (including those in figures and tables) are derived from previously published studies, which have been appropriately cited throughout the manuscript. Therefore, no new data were generated or analysed as part of this study.

References

1 P. R. Sihombing, *Int. J. Econ. Sci. Education*, 2026, **3**, 1–9.
2 S. Alone, S. Satputaley, D. Borkar, N. Bhave and M. Dudek, *Energies*, 2026, **19**, 909.
3 M. Walle, K. Yeneneh and G. Sufe, *Sci. Rep.*, 2025, **15**, 25516.
4 M. A. Balpande, M. M. Katiya, M. G. Dhonde and J. M. Gajbhiye, *Tetrahedron Green Chem.*, 2025, **5**, 100074.
5 T. M. M. Abdellatief, M. K. M. Handawy, A. Kamel, H. M. Abdelmotalib, A. Mustafa, F. Jamil, X. Duan, T. Salameh, A.-K. Hamid and M. Hussein, *Results Eng.*, 2025, **26**, 105347.
6 A. M. Ansari, F. A. Solangi, A. N. Sanjrani, F. Hussain, B. Zhang, Z. Ding and N. M. Nawi, *Results Eng.*, 2026, 108975.
7 V. Thakur, A. Chalana and N. Capalash, in *Biotechnology Innovations for a Sustainable Future: Integrating Clean Energy, Life on the Planet, Clean Water, and Climate Action*, Springer, 2026, pp. 2277–2288.
8 N. Fatima, N. Khanam, R. Kumari, V. C. Joshi and S. Bhattacharya, *Bioenergy Res.*, 2025, **18**, 40.
9 Y. Delhiwala, S. M. Y. Kosuru, P. B. Koorla and M. Mekala, *Chem. Prod. Process Model.*, 2026, DOI: 10.1515/cppm-2025-0045.
10 Z. Yılbaşı, *Sustainability*, 2025, **17**, 6145.
11 A. L. Olson, *Beyond Ethanol and Biodiesel: the Potential of Glycerol Derivatives and C_1–C_4 Alcohols for Motor Fuel Applications*, Lund University, 2024.
12 H. M. Saleh and A. I. Hassan, *Appl. Chem. Eng.*, 2024, **7**, 2084.
13 S. Ghasemi, I. Sadeghkhani and M. Parhamfar, *Solar Compass*, 2026, **17**, 100157.
14 M. S. Su'ait, N. A. Ludin and K. Sopian, in *Renewable Energy Technologies and Strategies in the Global Energy Transition*, ACS Publications, 2025, pp. 1–14.
15 P. Laskowski and M. Zimakowska-Laskowska, *Combust. Engines*, 2025, **201**, 129–135.
16 J. N. Nair, T. S. Rao, M. B. S. S. Reddy, V. D. Raju, H. Venu, A. A. Hadi, A. Smerat, T. M. Y. Khan, A. S. Shaik and M. A. Khan, *RSC Adv.*, 2026, **16**, 6338–6365.
17 K. Yeneneh and G. Sufe, *PLoS One*, 2026, **21**, e0341627.
18 G. Dhamodaran, G. S. Esakkimuthu, T. Palani and A. Sundaraganesan, *Emergent Mater.*, 2023, **6**, 1393–1413.
19 B. Rekha and R. Saravanathamizhan, *Int. J. Energy Res.*, 2021, **45**, 4508–4518.
20 S. Rajendran, A. Al-Samydai, G. Palani, H. Trilaksana, T. Sathish, J. Giri, R. Saravanan, J. I. J. Lalvani and F. Nasri, *Eng. Rep.*, 2025, **7**, e70108.
21 C. M. Igwebuike, S. Awad and Y. Andrès, *Molecules*, 2024, **29**, 1619.
22 S. Dutta, *Energy Fuels*, 2023, **37**, 2648–2666.
23 A. Manupathi, S. Gundekari, S. P. Thurlapati, M. Varkolu, R. Mudhulkar, S. K. Karmee and K. Ravi, *Catal. Surv. Asia*, 2026, 1–31.
24 L. Ramos, J. J. Ascencio, J. Villar, M. M. Cruz-Santos and A. K. Chandel, *Biofoundry Techniques for Biotechnology Applications*, 2026, pp. 1–25.
25 L. Wei, L. O. Pordesimo, C. Igathinathane and W. D. Batchelor, *Biomass Bioenergy*, 2009, **33**, 255–266.
26 M. M. Devadiga, A. S. Bhat, S. Sarangi, M. Osial, K. Joseph, S. J. Olusegun, J. Singh, N. Wang, L. A. R. Junior and S. K. Tiwari, *Energy Environ. Sci.*, 2026, **19**, 743–790.
27 A. E. K. Afedzi, G. S. Afrakomah, K. Gyan, J. Khan, R. Seidu, T. Baidoo, I. N. Sultan, A. K. Tareen and P. Parakulsuksatid, *Sustainability*, 2025, **17**, 499.
28 A. Kazmi, T. Sultana, A. Ali, A. Nijabat, G. Li and H. Hou, *Energy Strategy Rev.*, 2025, **57**, 101634.
29 S. Sasmal, in *Hydrogen and Low-Carbon Fuels in Circular Bioeconomy: Assessment Methodologies, Production Technologies and Sector-specific Applications*, Springer, 2025, pp. 187–208.
30 M. Tabatabaei, M. Aghbashlo, M. Dehhaghi, H. K. S. Panahi, A. Mollahosseini, M. Hosseini and M. M. Soufiyan, *Prog. Energy Combust. Sci.*, 2019, **74**, 239–303.
31 S. Ghosh, R. Das and T. Thakur, in *Alcohol Production Processes and Their Utilisation in the Transport Sector*, Springer, 2025, pp. 161–197.
32 L. M. Rossi, J. M. R. Gallo, L. H. C. Mattoso, M. S. Buckeridge, P. Licence and D. T. Allen, *ACS Sustainable Chem. Eng.*, 2021, **9**, 4293–4295.
33 A. Shukla, D. Kumar, M. Girdhar, A. Kumar, A. Goyal, T. Malik and A. Mohan, *Biotechnol. Biofuels Bioprod.*, 2023, **16**, 1–33.
34 K. Sajid, M. Rehan and A. S. Nizami, *Processes*, 2025, **13**, 1–26.
35 Z. Hamden, Y. El-Ghoul, F. M. Alminderej and H. Majdoub, *Waste Biomass Valorization*, 2025, 1–35.
36 S. Pimenow, O. Pimenowa, L. Moldavan, L. Udova, M. Wasilewski and N. Wasilewska, *Energies*, 2025, **18**, 1212.
37 M. Parvez, S. Lal, O. Khan, M. Ahmad, S. Lal Meena and B. L. Salvi, *Biofuels*, 2025, **16**, 638–651.
38 A. Kumar and S. Prajapati, *Solar-Powered Urbanization for a Sustainable Future*, CRC Press, 2026.
39 B. Oberle, S. Bringezu, S. Hatfield-Dodds, S. Hellweg, H. Schandl and J. Clement, *Global resources outlook: 2019*, International Resource Panel, United Nations Environment, Paris, France, 2019.
40 T. Chaturvedi, A. I. Torres, G. Stephanopoulos, M. H. Thomsen and J. E. Schmidt, *Energies*, 2020, **13**, 1493.
41 M. S. Sampaio, M. T. Lima, R. Wojcieszak and I. Itabaiana Jr, *ChemistrySelect*, 2025, **10**, e03106.
42 M. Guo, *Practices and Perspectives in Sustainable Bioenergy*, ed. M. Mitra and A. Nagchaudhuri, Springer India, New Delhi, 2020, pp. 29–56.

43 M. A. Ismael, M. El-Adawy, A. S. Farooqi, M. Hamdy, M. Z. Shahid, Z. Elserfy and M. A. Nemitallah, *Energy Fuels*, 2025, **39**, 13848–13878.
44 C. Angelici, B. M. Weckhuysen and P. C. A. Bruijnincx, *ChemSusChem*, 2013, **6**, 1595–1614.
45 C. R. V. Matheus, L. H. Chagas, G. G. Gonzalez, E. Falabella, S. Aguiar and L. G. Appel, *ACS Catal.*, 2018, **8**, 7667–7678.
46 J. M. R. Gallo, J. Bueno and U. Schuchardt, *J. Braz. Chem. Soc.*, 2014, **25**, 2229–2243.
47 T. Toda, Y. Sasakawa, H. Toda, K. Takenaka, K. Nishii and Y. Nakamura, *J. Appl. Polym. Sci.*, 2025, **142**, e56921.
48 M. Zanon-Zotin, C. Bergman-Fonte, T. Nogueira Morais, P. L. Barbosa Maia, L. Carvalho, G. Angelkorte, A. C. Oliveira Fiorini, P. Rua Rodriguez Rochedo, J. Portugal-Pereira, A. Szklo and R. Schaeffer, *J. Cleaner Prod.*, 2023, **428**, 139376.
49 J. N. Campos and J. E. Viglio, *MRS Energy Sustain.*, 2022, **9**, 35–48.
50 D. Zanchet, J. B. O. Santos, S. Damyanova, J. M. R. Gallo and J. M. C. Bueno, *ACS Catal.*, 2015, **5**, 3841–3863.
51 C.-Y. Wu and H.-S. Wu, *ACS Omega*, 2017, **2**, 4287–4296.
52 P. Kerdnoi, C. Autthanit, N. Chitpong and B. Jongsomjit, *Bull. Chem. React. Eng. Catal.*, 2020, **15**, 96–103.
53 H. M. Gobara, R. S. Mohamed, S. A. Hassan, F. H. Khalil and M. S. El-Sall, *Catal. Lett.*, 2016, **146**, 1875–1885.
54 C. A. Trickett, T. M. O. Popp, J. Su, C. Yan, J. Weisberg, A. Huq, P. Urban, J. Jiang, M. J. Kalmutzki and Q. Liu, *Nat. Chem.*, 2019, **11**, 170–176.
55 P. Iadrat, N. Horii, T. Atithep and C. Wattanakit, *ACS Appl. Mater. Interfaces*, 2021, **13**, 8294–8305.
56 A. Boretti, *Top. Catal.*, 2025, 1–21.
57 N. Nishimura and M. Tojo, *Phys. Chem. Chem. Phys.*, 2021, **23**, 822–826.
58 Y. Wang, H. Wang, T. She, R. Wang, Z. Xu, Q. Ji, S. Yang, L. Zhang and H. He, *Sep. Purif. Technol.*, 2025, **359**, 130859.
59 C. R. Kirman, A. A. Li, P. J. Sheehan, J. S. Bus, R. C. Lewis and S. M. Hays, *J. Toxicol. Environ. Health, Part B*, 2021, **24**, 1–29.
60 K. Sadeghi, Y. Lee and J. Seo, *Food Rev. Int.*, 2021, **37**, 155–176.
61 C. Schneider, R. Langer, D. Loveday and D. Hair, *J. Controlled Release*, 2017, **262**, 284–295.
62 M. S. Thompson, T. P. Vadala, M. L. Vadala, Y. Lin and J. S. Riffle, *Polymer*, 2008, **49**, 345–373.
63 W. H. Faveere, S. Van Praet, B. Vermeeren, K. N. R. Dumoleijn, K. Moonen, E. Taarning and B. F. Sels, *Angew. Chem.*, 2021, **133**, 12312–12331.
64 Z. Wu, J. Zhang, Z. Su, P. Wang, T. Tan and F.-S. Xiao, *Ind. Eng. Chem. Res.*, 2020, **59**, 17300–17306.
65 A. Mohsenzadeh, A. Zamani and M. J. Taherzadeh, *ChemBioEng Rev.*, 2017, **4**, 75–91.
66 J. Caraballo-Bello, J. L. Rodríguez-Lugo, D. Cabrera-Gallardo, F. M. Baena-Moreno and F. Vidal-Barrero, *Biomass Bioenergy*, 2026, **209**, 108963.
67 D. D. Kapoor, P. Madaan, J. Kumar, S. K. Tiwari, K. K. Gupta and R. K. Gupta, *J. Polym. Res.*, 2025, **32**, 345.
68 A. Mohsenzadeh, A. Zamani and M. J. Taherzadeh, *ChemBioEng Rev.*, 2017, **4**, 75–91.
69 A. Mohsenzadeh, A. Zamani and M. J. Taherzadeh, *ChemBioEng Rev.*, 2017, **4**, 75–91.
70 M. L. Derrien, in *Catalytic Hydrogenation: Studies in Surface Science and Catalysis*, ed. L. Cerveny, Elsevier, 1986, vol. 27, pp. 613–666.
71 I. Amghizar, J. N. Dedeyne, D. J. Brown, G. B. Marin and K. M. Van Geem, *React. Chem. Eng.*, 2020, **5**, 239–257.
72 R. Klaimi, S. Y. Alnouri, A. Miladinović and M. Stijepović, *Case Stud. Chem. Environ. Eng.*, 2026, **13**, 101323.
73 D. Grierson, *Annual Plant Reviews, The Plant Hormone Ethylene*, 2012, vol. 44, pp. 21–42.
74 D. Meng, L. Shen, R. Yang, X. Zhang and J. Sheng, *Biochim. Biophys. Acta, Gen. Subj.*, 2014, **1840**, 120–128.
75 C. Autthanit, C. Khaochartchai, P. Praserthdam and B. Jongsomjit, *Catal. Commun.*, 2021, **148**, 106169.
76 M. Limlamthong, N. Chitpong and B. Jongsomjit, *Bull. Chem. React. Eng. Catal.*, 2019, **14**, 1–8.
77 M. Dai, F. Yang, Z. Zhang, G. Liu and X. Feng, *J. Cleaner Prod.*, 2021, **310**, 127426.
78 Z. Zhao, Z. Zhang, P. Hao, C. Chen, Y. Liu, Y. Liu, X. Li and F. Wang, *ACS Sustainable Chem. Eng.*, 2025, **13**, 14770–14781.
79 J.-P. Han, H. Fang, H. Huang, Z.-Y. Su, H. Wang, B. Zhang, M. J. Zaworotko, S.-Q. Wang, M.-H. Yu, Z. Chang and X.-H. Bu, *Natl. Sci. Rev.*, 2026, **13**, nwaf548.
80 J. Sarfraz, T. Gulin-Sarfraz, J. Nilsen-Nygaard and M. K. Pettersen, *Nanomaterials*, 2021, **11**, 10.
81 W. Wu, H. Hu and D. Ding, *Cell Rep. Phys. Sci.*, 2021, **2**, 100405.
82 G. Issayev, B. R. Giri, A. M. Elbaz, K. P. Shrestha, F. Mauss, W. L. Roberts and A. Farooq, *Proc. Combust. Inst.*, 2021, **38**, 499–506.
83 L. Aguado-Deblas, J. Hidalgo-Carrillo, F. M. Bautista, D. Luna, C. Luna, J. Calero, A. Posadillo, A. A. Romero and R. Estevez, *Energies*, 2020, **13**(7), 1542.
84 D. C. Rakopoulos, *Fuel*, 2013, **105**, 603–613.
85 M. Zhang and Y. Yu, *Ind. Eng. Chem. Res.*, 2013, **52**, 9505–9514.
86 J. Worstell, *Adiabatic fixed-bed reactors: practical guides in chemical engineering*, Butterworth-Heinemann, Boston, 2014, pp. 81–108.
87 S. Hafeez, E. Pallari, G. Manos and A. Constantinou, in *Plastics Design Library, Plastics to Energy*, ed. S. M. Al-Salem, William Andrew Publishing, 2019, pp. 147–172.
88 R. d. B. S. Guerrero, C. E. D. dos Santos, L. A. Soares and M. Zaiat, *Biochem. Eng. J.*, 2020, **162**, 107716.
89 F. Maqbool, S. Z. Abbas, S. Ramirez-Solis, V. Dupont and T. Mahmud, *Int. J. Hydrogen Energy*, 2021, **46**, 5112–5130.
90 Y. Ju, H.-T. Oh, J.-C. Lee and C.-H. Lee, *Chem. Eng. J.*, 2021, **410**, 127414.
91 F. Fernandes and L. Lona, *Braz. J. Chem. Eng.*, 2000, **17**, 163–170.
92 F. Winter and B. Schratzer, in *Woodhead Publishing Series in Energy: Fluidized Bed Technologies for Near-Zero Emission*

Combustion and Gasification, ed. F. Scala, Woodhead Publishing, 2013, pp. 1005–1033.
93 M. N. Latif, W. N. Wan Isahak, A. Samsuri, S. Z. Hasan, W. N. Manan and Z. Yaakob, *Catalysts*, 2023, **13**(7), 1093.
94 A. M. Alkadhem, E. Perez-Botella, S. Pietsch-Braune, H. O. Mohamed, C. A. Grande, S. Heinrich and P. Castaño, *ChemCatChem*, 2026, **18**, e01109.
95 L. Wang, T. Zhou, B. Hou, H. Yang, N. Hu and M. Zhang, *Fluids*, 2025, **10**(6), 147.
96 M. Deshmukh, T. R. Kothawade, A. Pathan, U. S. Behera, J. S. Sangwai and H.-S. Byun, *Korean J. Chem. Eng.*, 2026, 1–38.
97 C. Zhu, Y. Zhang, X. Zhou, F. Kong and G. Jiang, *J. Therm. Anal. Calorim.*, 2021, **42**, 1–14.
98 A. S. Müller, L. M. Alfes, M. Fechtelkord and M. Muhler, *ChemSusChem*, 2026, **19**, e202501925.
99 H. Bateni and C. Able, *Catal. Ind.*, 2019, **11**, 7–33.
100 R. Chauhan, R. Sartape, N. Minocha, I. Goyal and M. R. Singh, *Energy Fuels*, 2023, **37**, 12589–12622.
101 S. S. Yang and Ö. L. Gülder, *Combust. Flame*, 2021, **225**, 39–47.
102 Y. Zhu, Z. Jin and W. Shen, in *DGMK International Conference on Catalysis - Innovative Applications in Petrochemistry and Refining*, 2011, pp. 61–64.
103 R. Suerz, K. Eränen, N. Kumar, J. Wärnå, V. Russo, M. Peurla, A. Aho, D. Yu. Murzin and T. Salmi, *Chem. Eng. Sci.*, 2021, **229**, 116030.
104 X. Xu, C. De Almeida and M. J. Antal, *J. Supercrit. Fluids*, 1990, **3**, 228–232.
105 V. Butera, Y. Tanabe, Y. Shinke, T. Miyazawa, T. Fujitani, M. Kayanuma and Y.-K. Choe, *Int. J. Quantum Chem.*, 2021, **121**, e26494.
106 J. F. DeWilde, C. J. Czopinski and A. Bhan, *ACS Catal.*, 2014, **4**, 4425–4433.
107 R. L. Madan, *Organic Reactions, Conversions, Mechanisms and Problems (An Organic Chemistry Handbook)*, S. Chand & Company Pvt. Ltd, New Delhi, 4th edn, 2014.
108 T. K. Phung and G. Busca, *Chem. Eng. J.*, 2015, **272**, 92–101.
109 I. K. M. Yu, H. Chen, F. Abeln, H. Auta, J. Fan, V. L. Budarin, J. H. Clark, S. Parsons, C. J. Chuck, S. Zhang, G. Luo and D. C. W. Tsang, *Crit. Rev. Environ. Sci. Technol.*, 2021, **51**, 1479–1532.
110 A. W. Budiman, J. S. Nam, J. H. Park, R. I. Mukti, T. S. Chang, J. W. Bae and M. J. Choi, *Catal. Surv. Asia*, 2016, **20**, 173–193.
111 Y. Huang, B. Wang, H. Yuan, Y. Sun, D. Yang, X. Cui and F. Shi, *Catal. Sci. Technol.*, 2021, **11**, 1652–1664.
112 R. Himmelmann, E. Klemm and M. Dyballa, *Catal. Sci. Technol.*, 2021, **11**, 3098–3108.
113 M. Marosz, A. Kowalczyk and L. Chmielarz, *Catal. Today*, 2020, **355**, 466–475.
114 A. S. H. Makhlouf and G. A. M. Ali, *Waste Recycling Technologies for Nanomaterials Manufacturing*, Springer Nature, 2021, pp. 3–851, DOI: 10.1007/978-3-030-6831-2.
115 S. K. Tripathi, R. Kaur, H. Kaur, M. Rani, J. Kaur and H. Kaur, in *AIP Conference Proceedings*, American Institute of Physics, 2015, vol. 1661, p. 110027.
116 L. Ali, F. Subhan, M. Ayaz, S. S. ul Hassan, C. C. Byeon, J. S. Kim and S. Bungau, *Nanomaterials*, 2022, **12**, 1–23.
117 G. Rouhzad, S. J. Ahmadi, A. Charkhi, S. Ammari Allahyari and S. Sadjadi, *Sep. Sci. Technol.*, 2026, 1–12.
118 Z. Lu, Y. Wang, J. Cui, X. Bian, J. Tang, S. Wu and L. Wang, *J. Anal. Appl. Pyrolysis*, 2026, **195**, 107637.
119 N. Mustapha and M. Hjiri, *J. Sol-Gel Sci. Technol.*, 2026, **117**, 59.
120 W. Wang, W. Yu, Y. Tan, H. Yang, B. Li, X. Wang, X. Chen, L. Huang, Z. Sun, C. Zhong and W.-M. Lau, *J. Colloid Interface Sci.*, 2026, **710**, 140050.
121 M. Farooqui, A. Abid, R. Khan, F. Choudhary, P. Sharma, A. Safdar and H. Farooqi, *Discover Sens.*, 2026, **2**, 12.
122 Y. Zhao, A. S. Aydoğdu, S. F. Kurtoğlu-Öztulum and A. Uzun, *Chem.–Asian J.*, 2026, **21**, e00962.
123 S. Thambidurai, P. Gowthaman, M. Venkatachalam, S. Suresh and M. Kandasamy, *J. Alloys Compd.*, 2021, **852**, 156997.
124 S. Patil and S. Jagadale, in *Solution Methods for Metal Oxide Nanostructures*, ed. R. Mane, V. Jadhav and A. Al-Enizi, Elsevier, 2023, pp. 39–60.
125 P. P. Gedam and A. Jat, in *International e-Conference on Recent Trends in Material Science*, 2024, pp. 354–357.
126 A. Das and A. K. Ganguli, *RSC Adv.*, 2018, **8**, 25065–25078.
127 V. Maslova, E. A. Quadrelli, P. Gaval, A. Fasolini, S. Albonetti and F. Basile, *J. Environ. Chem. Eng.*, 2021, **9**, 105070.
128 C. Dhand, N. Dwivedi, X. J. Loh, A. N. Jie Ying, N. K. Verma, R. W. Beuerman, R. Lakshminarayanan and S. Ramakrishna, *RSC Adv.*, 2015, **5**, 105003–105037.
129 C. Dhand, N. Dwivedi, X. J. Loh, A. N. Jie Ying, N. K. Verma, R. W. Beuerman, R. Lakshminarayanan and S. Ramakrishna, *RSC Adv.*, 2015, **5**, 105003–105037.
130 M. M. ElFaham, A. M. Mostafa and E. A. Mwafy, *J. Phys. Chem. Solids*, 2021, **154**, 110089.
131 A. A. Belew and M. A. Assege, *Results Chem.*, 2025, **16**, 102438.
132 T. Q. Tazim, M. Kawsar, M. Sahadat Hossain, N. M. Bahadur and S. Ahmed, *Next Nanotechnol.*, 2025, **7**, 100167.
133 K. I. Nassar, S. S. Teixeira and M. P. F. Graça, *Gels*, 2025, **11**, 657.
134 S. A. Hassan, H. M. Gobara, M. M. Gomaa, R. S. Mohamed and F. H. Khalil, *RSC Adv.*, 2015, **5**, 54460–54470.
135 Z. Yin, S. Li, X. Li, W. Shi, W. Liu, Z. Gao, M. Tao, C. Ma and Y. Liu, *RSC Adv.*, 2023, **13**, 3265–3277.
136 S. A. Hassan, H. M. Gobara, M. M. Gomaa, R. S. Mohamed and F. H. Khalil, *RSC Adv.*, 2015, **5**, 54460–54470.
137 E. Vialkova, M. Obukhova and L. Belova, *Water*, 2021, **13**(13), 1784.
138 K. Baba, H. Kasai, K. Nishida and H. Nakanishi, in *Functional Organic Nanocrystals*, 2011, vol. 15, pp. 397–436.
139 K. Baba, H. Kasai, K. Nishida and H. Nakanishi, *Nanocrystals*, ed. Y. Masuda, IntechOpen, 2011, vol. 15, p. 397.
140 A. Mohammad, M. E. Khan, M. H. Cho and T. Yoon, *Ceram. Int.*, 2021, **47**, 15073–15081.

141 K. Selvakumar, T. H. Oh, Y. Wang, T. Sadhasivam, S. Sadhasivam and M. Swaminathan, *Chemosphere*, 2023, **341**, 140012.
142 B. Gielen, J. Jordens, L. C. J. Thomassen, L. Braeken and T. Van Gerven, *Crystals*, 2017, **7**, 1–20.
143 E. Amdeha, R. S. Mohamed and A. S. Dhmees, *Ceram. Int.*, 2021, **47**, 23014–23027.
144 H. M. Salem, *New Trends for Preparing Mesoporous Catalysts to Produce Green Fuel*, Ain Shams University, 2020, p. 238.
145 A. Kumar, *Ind. Eng. Chem. Res.*, 2021, **60**, 16561–16576.
146 J. Deng, X. Hu, A. J. Klaver, J. Liu, B. Liu, L. Bai, M. Xie and D. Zhang, *Chem. Rev.*, 2025, **125**, 11260–11357.
147 P. Lei, M. Liu, J. Wang and J. Chen, *ACS Catal.*, 2026, 4232–4265.
148 Y. Cho, L. M. Tran, S. J. Park, H.-K. Min and M. B. Park, *Mol. Catal.*, 2024, **564**, 114300.
149 H. R. Ali, R. S. Mohamed, M. F. Mubarak and A. El Shahawy, *Desalin. Water Treat.*, 2021, **227**, 42–57.
150 N. Thibanyane, J. Gorimbo and Y. Yao, *Advances on Catalyst Support Modification and their Effect on Fischer Tropsch Synthesis: A Review*, 2024.
151 N. Hijazi, A. Bavykina, I. Yarulina, T. Shoinkhorova, E. V Ramos-Fernandez and J. Gascon, *Chem. Soc. Rev.*, 2025, **54**, 6335–6384.
152 S. Lawson, K. Baamran, K. Newport, F. Rezaei and A. Rownaghi, *ACS Appl. Mater. Interfaces*, 2021, **13**, 55198–55207.
153 H. M. Gobara, R. S. Mohamed and W. A. Aboutaleb, *Microporous Mesoporous Mater.*, 2021, **323**, 111151.
154 R. S. Mohamed, M. Bakry, W. A. Aboutaleb and H. M. Gobara, *Ceram. Int.*, 2024, **50**, 27771–27785.
155 K. Tian, Q. Li, W. Jiang, X. Wang, S. Liu, Y. Zhao and G. Zhou, *RSC Adv.*, 2021, **11**, 11952–11958.
156 F. Khanbolouk, F. Yazdani, M.-H. Fatemi and M. Y. Najafabadi, *Cost-Effective Synthesis of Gamma Alumina for Propane Dehydrogenation: A Study of Raw Materials, Process Optimization, and Catalyst Performance*, 2025.
157 B. Mezari, P. C. M. M. Magusin, S. M. T. Almutairi, E. A. Pidko and E. J. M. Hensen, *J. Phys. Chem. C*, 2021, **125**, 9050–9059.
158 D. Fan, D.-J. Dai and H.-S. Wu, *Materials*, 2013, **6**, 101–115.
159 H. M. Gobara, *Egypt. J. Pet.*, 2014, **23**, 105–118.
160 G. Chen, S. Li, F. Jiao and Q. Yuan, *Catal. Today*, 2007, **125**, 111–119.
161 N. Masiran, D. V. N. Vo, M. A. Salam and B. Abdullah, *Procedia Eng.*, 2016, **148**, 1289–1294.
162 H. Tayyab, S. Liu, H. Zhang, R. Shen, Y. Liu, J. Jiang and B. Li, *J. Mater. Chem. A*, 2026, DOI: 10.1039/d5ta07323e/v2/review1.
163 E. Guzmán, *ChemCatChem*, 2025, **17**, e202500522.
164 Y. Hasegawa, W. Matsuura, C. Abe and A. Ikeda, *Membranes*, 2021, **11**(5), 347.
165 B. Torres-Olea, A. Pérez-Merchán, P. Díaz-Maizkurrena, J. M. Requies, R. Moreno-Tost, J. A. Cecilia, C. García-Sancho and P. Maireles-Torres, *Catal. Today*, 2024, **427**, 114439.
166 J. Cho, Y. Yun, H. Xu, J. Sun, A. W. Burton, K. G. Strohmaier, G. Terefenko, H. Vroman, M. Afeworki, G. Cao, H. Wang, X. Zou and T. Willhammar, *Chem. Mater.*, 2021, **33**, 4146–4153.
167 H. Hayashi, A. P. Côté, H. Furukawa, M. O'Keeffe and O. M. Yaghi, *Nat. Mater.*, 2007, **6**, 501–506.
168 W. Lutz, R. A. Shutilov and V. Y. Gavrilov, *Z. Anorg. Allg. Chem.*, 2014, **640**, 577–581.
169 T. Cordero-Lanzac, A. T. Aguayo, A. G. Gayubo and J. Bilbao, *Fuel*, 2021, **302**, 121061.
170 Q. Sheng, K. Ling, Z. Li and L. Zhao, *Fuel Process. Technol.*, 2013, **110**, 73–78.
171 K. Gołąbek, K. A. Tarach, U. Filek and K. Góra-Marek, *Spectrochim. Acta, Part A*, 2018, **192**, 464–472.
172 A. Velty and A. Corma, *Chem. Soc. Rev.*, 2023, **52**, 1773–1946.
173 X. Chen, J. Huang and G. Yang, *Catalysts*, 2025, **15**, 204.
174 S. Mondal, S. Ruidas, S. Chongdar, B. Saha and A. Bhaumik, *ACS Sustainable Resour. Manage.*, 2024, **1**, 1672–1704.
175 C. Li, Z. Sun, Y. Wang, J. Zhu, J. Wu, L. Feng, X. Wen, W. Cai, H. Yu and M. Wang, *J. Energy Storage*, 2024, **95**, 112504.
176 Ł. Kuterasiński, U. Filek, M. Gackowski, M. Zimowska, M. Ruggiero-Mikołajczyk and P. J. Jodłowski, *Ultrason. Sonochem.*, 2021, **74**, 105581.
177 P. Vondrová, Z. Tišler, J. Kocík, H. de Paz Carmona and M. Murat, *React. Kinet., Mech. Catal.*, 2021, **132**, 449–462.
178 D. Masih, S. Rohani, J. N. Kondo and T. Tatsumi, *Microporous Mesoporous Mater.*, 2019, **282**, 91–99.
179 D. Janićijević, S. Uskoković-Marković, A. Popa, B. Nedić Vasiljević, A. Jevremović, M. Milojević-Rakić and D. Bajuk-Bogdanović, *Chem. Pap.*, 2021, **75**, 3169–3180.
180 H. Liu, J. Bao, S. Zen, Z. Chen, W. Lai, W. Fang, X. Yi and Q. Yang, *J. Mater. Chem. A*, 2025, **13**, 36468–36477.
181 J. Meng, F. Fang, N. Feng, H. Wan and G. Guan, *RSC Adv.*, 2020, **10**, 2472–2482.
182 L. Leonova, G. Pampararo, V. Vykoukal, L. Simonikova, F. Devred, P. Eloy, A. Styskalik and D. P. Debecker, *Catal. Today*, 2026, **461**, 115494.
183 T. K. Phung, L. Proietti Hernández, A. Lagazzo and G. Busca, *Appl. Catal., A*, 2015, **493**, 77–89.
184 A. Styskalik, I. Kordoghli, C. Poleunis, A. Delcorte, D. D. Dochain, Z. Moravec, J. Vida, T. Homola, C. Aprile, L. Fusaro, F. Devred and D. P. Debecker, *J. Mater. Sci.*, 2021, **56**, 14001–14018.
185 J. Lakshmidevi, V. Vakati, B. Ramesh Naidu, M. Raghavender, K. S. V. K. Rao and K. Venkateswarlu, *Sustainable Chem. Pharm.*, 2021, **19**, 100371.
186 N. S. Pagar, P. R. Karandikar, A. J. Chandwadkar and R. M. Deshpande, *J. Porous Mater.*, 2021, **28**, 423–433.
187 A. M. Eldeeb, W. A. Aboutaleb, R. S. Mohamed, A. S. Dhmees and A. I. Ahmed, *J. Energy Inst.*, 2022, **103**, 84–93.
188 A. J. Schwanke, R. Balzer and S. Pergher, in *Handbook of Ecomaterials*, ed. L. M. T. Martínez, O. V. Kharissova and B. I. Kharisov, Springer International Publishing, Cham, 2017, pp. 1–22.

189 G. Rajput, V. Gosu and V. Subbaramaiah, *J. Environ. Chem. Eng.*, 2025, 115634.
190 H. M. El Sharkawy, M. S. Sayed and R. S. Mohamed, *Sep. Purif. Technol.*, 2025, 134540.
191 R. E. Morsi and R. S. Mohamed, *R. Soc. Open Sci.*, 2018, **5**, 172021.
192 R. Rezvany, S. K. Hassaninejad-Darzi and S. M. Pourali, *Fuel Cells*, 2021, **21**, 301–316.
193 R. E. Morsi and R. S. Mohamed, *R. Soc. Open Sci.*, 2018, **5**, 172021.
194 S. Alahmadi, *Orient. J. Chem.*, 2012, **28**, 1–11.
195 M. C. A. Fantini, J. R. Matos, L. C. C. da Silva, L. P. Mercuri, G. O. Chiereci, E. B. Celer and M. Jaroniec, *Mater. Sci. Eng., B*, 2004, **112**, 106–110.
196 T. M. Albayati and A. M. Alkafajy, *Al-Khwarizmi Eng. J.*, 2019, **15**, 34–43.
197 T. M. Díez-Rodríguez, E. Blázquez-Blázquez, J. P. Lourenço, J. C. Martínez, M. L. Cerrada and E. Pérez, *Microporous Mesoporous Mater.*, 2025, **382**, 113391.
198 H. H. El-Maghrabi, R. S. Mohamed and A. A. Younes, *Environ. Sci. Pollut. Res.*, 2021, **28**, 45933–45945.
199 H. M. Salem, R. S. Mohamed, A. A. Alkahlawy, H. M. Gobara, A. E. A. Hassan and S. A. Hassan, *J. Porous Mater.*, 2019, **26**, 735–745.
200 H. M. Gobara, S. A. Hassan, A. M. A. El Naggar, R. S. Mohamed, A. A. Alkahlawy, A. A. Salem and H. M. Salem, *Int. J. Hydrogen Energy*, 2020, **45**, 24710–24725.
201 X. Dong, J. Tian, J. Lei and Y. Chen, *J. Environ. Chem. Eng.*, 2022, **10**, 107517.
202 I. Sobczak, J. Wisniewska, P. Decyk, M. Trejda and M. Ziolek, *Int. J. Mol. Sci.*, 2023, **24**(3), 2252.
203 V. V Sobornova and I. A. Khodov, *Phys. Chem. Chem. Phys.*, 2026, **28**, 3540–3549.
204 M. Crucianelli, B. M. Bizzarri and R. Saladino, *Catalysts*, 2019, **9**, 984.
205 Y.-W. Lin, T.-W. Cheng, K.-W. Lo, C.-Y. Chen and K.-L. Lin, *Microporous Mesoporous Mater.*, 2021, **310**, 110643.
206 H. M. Gobara, S. A. Hassan, A. M. A. El Naggar, R. S. Mohamed, A. A. Alkahlawy, A. A. Salem and H. M. Salem, *Int. J. Hydrogen Energy*, 2020, **45**, 24710–24725.
207 H. M. Salem, R. S. Mohamed, A. A. Alkahlawy, H. M. Gobara, A. E. A. Hassan and S. A. Hassan, *J. Porous Mater.*, 2019, **26**, 735–745.
208 G. Garbarino, R. Prasath Parameswari Vijayakumar, P. Riani, E. Finocchio and G. Busca, *Appl. Catal., B*, 2018, **236**, 490–500.
209 A. Styskalik, I. Kordoghli, C. Poleunis, A. Delcorte, C. Aprile, L. Fusaro and D. P. Debecker, *Microporous Mesoporous Mater.*, 2020, **297**, 110028.
210 G. Li, B. Wang, Z. Ma, H. Wang, J. Ma, C. Zhao, J. Zhou, D. Lin, F. He, Z. Han, Q. Sun and Y. Wang, *Commun. Chem.*, 2020, **3**, 1–13.
211 S. P. Naik, V. Bui, T. Ryu, J. D. Miller and W. Zmierczak, *Appl. Catal., A*, 2010, **381**, 183–190.
212 C. Krutpijit, P. Tochaeng and B. Jongsomjit, *Catal. Commun.*, 2020, **145**, 106102.
213 T. K. Phung and G. Busca, *Catal. Commun.*, 2015, **68**, 110–115.
214 A. Styskalik, V. Vykoukal, L. Fusaro, C. Aprile and D. P. Debecker, *Appl. Catal., B*, 2020, **271**, 118926.
215 B. A. Murray, in *Organic Reaction Mechanisms 2016*, 2020, pp. 1–70.
216 A. A. Gomaa, A. Abdelkader and M. Khodari, *Waste Biomass Valorization*, 2024, **15**, 4839–4851.
217 H. T. Abdulrazzaq and T. J. Schwartz, Catalytic conversion of ethanol to commodity and specialty chemicals, *Ethanol*, ed. A. Basile, A. Iulianelli, F. Dalena and T. N. B. T.-E. Veziroğlu, Elsevier, 2019, pp. 3–24.
218 A. R. Varma, M. Z. Rahman, S. Gadkari, A. Tawai, M. Sriariyanun, A. Xia, V. Kumar and S. K. Maity, *ChemSusChem*, 2026, **19**, e202501926.
219 Y. Cui, D. Wang, H. Ben, X. Su, X. Yang and Y. Huang, *Chem. Sci.*, 2026, **17**, 3449–3479.
220 F. Lin, M. Xu, K. K. Ramasamy, Z. Li, J. L. Klinger, J. A. Schaidle and H. Wang, *ACS Catal.*, 2022, **12**, 13555–13599.
221 W. Xia, F. Wang, X. Mu and K. Chen, *Fuel Process. Technol.*, 2017, **166**, 140–145.
222 W. Xia, Y. Zhang, C. Ma, Z. Jiang, X. Wang, K. Chen, D. Liu and Y. Wang, *Energy*, 2025, **319**, 135024.
223 Z. Jiang, W. Xia, Y. Zhang, X. Wang, M. Dong, K. Chen, D. Liu and B. Lu, *Clean Energy*, 2025, **9**, 115–127.
224 X. Li, S. Ma and H. Li, *Green Chem.*, 2022, **24**, 7243–7280.
225 M. Iwamoto, *Molecules*, 2011, **16**, 7844–7863.
226 T. K. Phung, T. L. M. Pham, K. B. Vu and G. Busca, *J. Environ. Chem. Eng.*, 2021, **9**, 105673.
227 E. Ebadzadeh, M. H. Khademi and M. Beheshti, *Chem. Eng. J.*, 2021, **405**, 126605.
228 A. Takahashi, W. Xia, Q. Wu, T. Furukawa, I. Nakamura, H. Shimada and T. Fujitani, *Appl. Catal., A*, 2013, **467**, 380–385.
229 D. Cheng, Y. Xiao, J. Yuan, D. Fan, N. Chen, J. Han, S. Liu, A. Zheng, P. Tian and Z. Liu, *J. Am. Chem. Soc.*, 2025, **148**, 1801–1811.
230 J. Lara Monsibais, C. Valero Luna, A. Bañuelos Frías, L. A. Romero De León, L. O. Solis Sánchez, M. d. R. Martínez Blanco and L. Alvarado Perea, *Int. J. Chem. React. Eng.*, 2025, DOI: 10.1515/ijcre-2025-0136.
231 R. J. Dhanorkar, S. Mohanty and V. K. Gupta, *Ind. Eng. Chem. Res.*, 2021, **60**, 4517–4535.
232 X. Li, Y. Zhao, J. Pang, P. Gao, M. Zheng and G. Hou, *ACS Catal.*, 2025, **15**, 5053–5085.
233 N. Liu, L. Zhang, K. Wang, L. Shao, X. Guo, Y. He, Z. Wu, P. Zhan, G. Liu, J. Wu, G. Yang and N. Tsubaki, *Appl. Surf. Sci.*, 2022, **602**, 154299.
234 M. V. Singh, M. Sethi, S. Srivastav, K. Stanikzai, A. Chauhan, D. Pan, Z. Guo, I. Seok, A. Pereira and S. Tanwar, *ES Energy Environ.*, 2024, **24**, 1–16.
235 Y. Qi, Z. Liu, S. Liu, L. Cui, Q. Dai, J. He, W. Dong and C. Bai, *Catalysts*, 2019, **9**(1), 97.
236 H. Li, J. Pang, N. R. Jaegers, L. Kovarik, M. Engelhard, A. W. Savoy, J. Hu, J. Sun and Y. Wang, *J. Energy Chem.*, 2020, **54**, 7–15.

237 A. S. Fedotov, V. I. Uvarov, M. V Tsodikov, I. I. Moiseev, S. Paul, S. Heyte, P. Simon, M. Marinova and F. Dumeignil, *Kinet. Catal.*, 2020, **61**, 390–404.
238 Y. Zhao, X. Li, J. Pang, W. Yu, P. Yan, Y. Su, L. Li and M. Zheng, *Chem. Eng. J.*, 2025, **519**, 164837.
239 H. Deng, F. Luo, G. Feng, R. Zhang and R. Ye, *Carbon Hydrogen*, 2025, **27**, 401–419.
240 E. V. Makshina, W. Janssens, B. F. Sels and P. A. Jacobs, *Catal. Today*, 2012, **198**, 338–344.
241 H. Ma, S. Zhang, H. Gao and D. Wen, *Catalysts*, 2025, **15**, 791.
242 N. Kaur and N. Banik, in *Solid Base Catalysts*, 2024, pp. 169–231.
243 R. Lei, Z. Chen, Q. Xu, N. Wang, Y. Qin, T. Wang, X. Lin and X. Qiu, *Green Chem.*, 2025, **27**, 9643–9662.
244 Y. Ma, S. Liu, X. Han, L. Ye, H. Xu, L. Kong, J. Li, X. Pu and J. Liu, *ACS Sustain. Chem. Eng.*, 2026, **14**, 1467–1476.
245 T. Saulnier-Bellemare and G. S. Patience, *ACS Omega*, 2024, **9**, 23121–23137.
246 X. Lan, J. G. Chen and T. Wang, *Chem. Soc. Rev.*, 2025, **54**, 7654–7705.
247 X. Lin, X. Fei, D. Chen, Y. Qi, Q. Xu, Y. Liu, Q. Zhang, S. Li, T. Wang and Y. Qin, *ACS Catal.*, 2022, **12**, 11573–11585.
248 X. Fei, Q. Xu, L. Xue, X. Zhong, Z. Zhang, K. Liu, X. Lin, T. Wang, Y. Qin and X. Qiu, *Ind. Eng. Chem. Res.*, 2021, **60**, 17959–17969.
249 Q. Xu, X. Fei, X. Qiu, X. Wang, T. Wang, X. Lin, S. Li and Y. Qin, *Chem. Eng. J.*, 2024, **489**, 151092.
250 P. Lakhani, D. Bhanderi and C. K. Modi, *J. Nanopart. Res.*, 2024, **26**, 148.
251 R. Zhang, J. Zhang, H. Liu, Z. Jiang, X. Liu, W. Wang, L. Peng and C. Hu, *ACS Catal.*, 2024, **14**, 5167–5197.